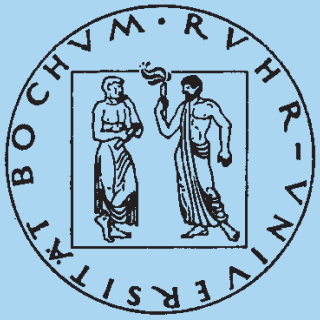

RUHR-UNIVERSITÄT BOCHUM

W. Tampczynski

Strain history effect in cyclic plasticity

Heft Nr. 52

Mitteilungen
aus dem
Institut für Mechanik

Institut für Mechanik
RUHR-UNIVERSITÄT BOCHUM

W. Trampczynski

Strain history effect in cyclic plasticity

Mitteilungen aus dem Institut für Mechanik Nr. 52
Juli 1987

Herausgeber:

Institut für Mechanik der Ruhr-Universität Bochum

 Dr. W. Trampczynski
Institute of Fundamental Technological Research
Polish Academy of Science
07.1986 - 09.1986 Stipendiat der Alexander von Humboldt-Stiftung an der Ruhr-Universität Bochum

Abstract

The simple plastic shear, plastic torsion, cyclic plastic shear, cyclic plastic tension - torsion and out of phase tests of 18G2A steel were performed. The specimens were loaded monotonically and cyclically with constant effective strain rate under controlled amplitude of plastic strains at room temperature. Using the technique of succesive unloadings (presented in [12]), the standard physical quantities and the stress jumps corresponding to opposite directions of plastic straining were measured. For the Huber - Mises yield surface such results enable to follow the evolution of kinematic and isotropic hardening for such programs. The obtained results shows new effects concerning the influence of strain history on cyclic plasticity. They are similar to that obtained for 21CrMoV57 steel [12] and can be used for verification of existing theoretical approaches.

Zusammenfassung

In dieser Arbeit werden die einfache plastische Scherung, plastische Torsion, zyklische plastische Scherung, zyklische Zug-Torsion und 'out of phase'-Experimente an einem 18G2A-Stahl untersucht. Die Proben wurden monoton bzw. zyklisch mit konstanter effektiver Verzerrungsgeschwindigkeit unter kontrollierter Dehnungsamplitude bei Raumtemperatur belastet.

Mittels der Methode der sukzessiven Entlastungen (vgl. [12]) wurden die Spannungssprünge bei entgegengesetzten plastischen Verzerrungen gemessen.

Diese Ergebnisse ermöglichen für eine Huber-Mises-Fließfläche die Ermittlung der Evolution von isotroper und kinematischer Verfestigung.

Die erhaltenen Ergebnisse zeigen neue Effekte bezüglich des Einflusses der Verzerrungsgeschichte bei zyklischer Plastizität.
Sie sind ähnlich den in [12] für den Stahl 21CrMoV57 ermittelten Resultaten und können für die Verifikation bestehender theoretischer Ansätze genutzt werden.

Contents

1.Introduction

The behaviour of solids under monotonic and cyclic plastic loading is very complex and even more complex when the strain history effects are taken into account. Since an anticipation of such behaviour for metals plays an important practical role there were proposed a lot of theories to describe it. Some of them [1-4] are based upon the assumption that, apart from traditional yield surface in the stress space, there exist one or more surfaces in a space of the tensors describing the motion of the centre of the yield surface. The evolution laws for the kinematic and the isotropic part of hardening are usually postulated first and then they are jointly verified by means of the data obtained from the measurements of global strain - stress curves. Such data are insufficient for unique separation of, mentioned above, two hardening components. They have been performed also the experimental investigations concerning the possible shape of yield surfaces and its properties under simple loading programs and under cyclic loading [5-11]. The position and the shape of the yield surface were determined only at some chosen instants of a cyclic loading programs. The obtained results are still insufficient for satisfactory verification of the law of kinematic and isotropic hardening. So, for proper formulation of such concepts, there are required new experimental data giving the measurements of some aditional quantity not only in some chosen points of strain history, but during all cyclic loading program, also inside single cycle. Such results are shown in [12] for 21CrMoV57 steel under tension - compresion and pure torsion cyclic loading at room temperature. They were obtained using the new technique of succesive unloadings.

The objective of this work is to verify those results for different material (18G2A steel) and to provide the new experimental data for another strain histories.

2.Experimental technique.

The evolution of yield surface center and the evolution of yield surface radius, during monotonic and plastic loading, were determined using the tehnique of succesive unloadings. The detail description of this procedure is given in [12] and now the only main idea will be presented.

Let us denote by the deviatoric part of stress tensor σ_{ij}, $S_{ij} = \sigma_{ij} - \delta_{ij}\sigma_{kk}/3$. Most of the theoretical models in cyclic plasticity employ the notion of a yield function f, which can be written in the following form:

$$f(S_{ij} - \alpha_{ij}, H) = 0, \quad f(0,H) \leq 0 \tag{1}$$

where $\alpha_{ij}(\alpha_{kk}=0)$ is sometimes identified with a macroscopic measure of microstresses. The letter H denotes symbolically the set of other possible parameters which describe the history of plastic strains.

Let us discuss the basic program O-C of proportional plastic straining shown in Fig.1a. The program is interupted at point A where the specimen is unloaded and reloaded into reverse direction until the conventional small value η (for instance $\eta = 0.000005$) of the increment of e^P is achieved. Then, the former direction of plastic strain is applied. In such a way one can, in an experimental program, identify the stress vector S^R_{ij} (Fig.1b). Its one end lies at the yield surface at point B' where plastic strain - rate vector has the direction opposite to that prescribed in the basic program. The value of S^R_{ij}, in chosen moment of the strain history, is those aditional physical quantity, mentioned in introduction, useful for stisfactory verification of the kinematic and isotropic hardening at point A.

Let us denote:

$$Y_{ij} = (S_{ij} - S^R_{ij})/2, \quad \Pi_{ij} = (S_{ij} + S^R_{ij})/2 \tag{2}$$

It is possible to show, that for yield surface approximated by the Huber - Mises sphere (the length of radius R is independent on n_{ij})

$$Y_{ij} = n_{ij}R(H), \qquad \Pi_{ij} = \alpha_{ij} \tag{2a}$$

where n_{ij} - unit "vector" of directions in S_{ij} space.

Considering the projection of Π_{ij} and Y_{ij} onto the plastic straining direction (m_{ij} - the unit "vector" describing the plastic straining direction, $n_{ij}=m_{ij}(\text{sgn } e^p)$):

$$Y = |Y_{ij}m_{ij}| = |(S_{ij} - S^R_{ij})m_{ij}|/2 \geq 0 \tag{3}$$

$$\Pi = {}_{ij}m_{ij} = (S_{ij} + S^R_{ij})m_{ij}/2$$

The interpretation of Y_{ij} and Π_{ij} follows from (2a):

$$Y = |m_{ij}n_{ij}|R, \qquad \Pi = \alpha_{ij}m_{ij} \tag{3a}$$

Thus Π is the projection of α_{ij} on the direction m_{ij}, whereas Y equals the principal radius of an ellipsoide whenewer $|m_{ij}n_{ij}| = 1$.

It means, that having S_{ij} and S^R_{ij} values in proportional loading proces, and assuming the Huber - Mises yield criterion, it is possible to define the yield surface center and the yield surface radius at chosen points of the plastic strain history. Because of simplicity of this technique, many points can be investigate (also, for instance, inside single cycle) and the evolution laws for kinematic and isotropic hardening can be experimentally defined.

In Fig.2 it is shown the application of the unloading technique for monotonic torsion. The specimen was loaded by torsion with the constant effective strain rate $e^p_e = 3.4\times 10^{-4}/s$. After every effective plastic strain increment $\Delta\varepsilon^p_e=0.008$ the stress tensor value S_{ij} was taken into memory, and the torque changes its direction to opposite. The slope of the unloading curve was measured. At point B (due to rheological effects) it was equal to the Young modulus for the virgin material and straight line "a" of the same slope was determined. The distance between the succesive points at the unloading curve (or loading in "opposite" direction) and this line was then calculated. When it was equal to the

"offset definition" the another yield point S^R_{ij} was found and the torque changed its direction to the initial one. Having S_{ij} and S^R_{ij}, in the chosen points of strain history, the yield surface radius (Y) and the yield surface center (Π) was determined according to (3). Similar way such a values were found also for cycling loading even inside the single cycle.

The objective of this paper is the experimental determination of Y_1 and Π_1, during cyclic and monotonic loading of a specimen under controlled plastic strain. The experiments concern three cases:

a)simple plastic shear,

$$\Pi_1 = \sqrt{(3/2)}\Pi = \sqrt{3}\ (\tau + \tau^R)/2 \qquad (4)$$
$$Y_1 = \sqrt{(3/2)}Y = \sqrt{3}\ |(\tau - \tau^R)|/2$$

b)simple plastic tension (compresion),

$$\Pi_1 = \sqrt{(3/2)}\Pi = (\sigma + \sigma^R)/2 \qquad (5)$$
$$Y_1 = \sqrt{(3/2)}Y = |(\sigma - \sigma^R)|/2$$

where $\Pi_1 = \sqrt{(3/2)}\Pi$ and $Y_1 = \sqrt{(3/2)}Y$.

c)out of phase plastic loading.

The experimental programs were performed at room temperature on thin tubes (outer diameter 24 mm., wall thickness 2 mm., gauge length 38 mm.) made of 18G2A steel. Tension - compresion and torsion in opposite directions of cyclic programs were made using the Schenck tension - compresion - torsion machine connected "on line" with the HP 1000 computer (machine and computer sponsored by Stiftung Volkswagenwerk). Force and moment acting on the specimen, elongation and torsion of the specimen, and other possible 35 measurements were read by a computer, then elaborated and the results obtained were used for continuous machine control. In this case it was symmetric cyclic program for fixed plastic strain amplitude with a set of unloadings (loading in opposite direction in order to determine the opposite point of the yield surface). All programs were performed at a constant effective strain rate $e^p_e = 3.4\ 10^{-4}/s$, and the actual stresses versus the logarithmic plastic strain coordinates were calculated and plotted

($\varepsilon=\ln(1/1_o)$, $\sigma=P/F_a$, where 1_o - gauge length, F_a - current specimen cross - section, P - force). Yielding was determined by the offset definition of = 0.0005, what was discussed before.

3.Experimental results

Experiment 1. Monotonic torsion with unloadings.

The specimen was loaded by torsion at the constant effective strain rate $e^p_e=3.4\times10^{-4}/s$. After every effective plastic strain increment $\Delta\varepsilon^p_e=0.008$, the unloading technique was used to determine the position of yield surface center (assuming the Huber - Mises yield criterion) and the yield surface radius. This way it was possible to establish the loading path for both Π_1 and Y_1 (Fig.3).

Experiment 2. Monotonic tension with unloadings.

The specimen was loaded by tension with this same effective strain rate as in Experiment 1. Using the similar experimental technique the loading path for Π_1 and Y_1 was established (Fig.4).

Experiment 3. Cyclic torsion with following plastic strain amplitudes $\gamma^p/\sqrt{3} = \pm0.005, \pm0.010, \pm0.015, \pm0.020 \pm0.030, \pm0.005$

The specimen was cyclically loaded with gradually increasing plastic strain amplitude $\gamma^p/\sqrt{3}=\pm0.005$ - ±0.030 and than the amplitude $\gamma^p/\sqrt{3}=\pm0.005$ was applied. Every strain amplitude change took place after reaching the steady state cycle for the former amplitude value. Using the unloading technique, the yield surface center movement and the evolution of yield surface radius for the first cycle and for the steady loop at every atrain amplitude was

defined.

In Fig.5 are shown the stress-plastic strain curves (thick lines) and the Π_1 curves (thin lines) for increasing strain amplitudes $\gamma^p/\sqrt{3}=\pm 0.005-\pm 0.030$. The solid lines are drawn for the first cycle for certain amplitude and the dashed one for the stabilized loop.

In Fig.6 there are compared the stress - plastic strain curves, the Π_1 curves and the Y_1 curves for strain amplitude $\gamma^p/\sqrt{3}=\pm 0.005$ for virgin material (Fig.6a) and for material with history of growing plastic strain amplitudes $\gamma^p/\sqrt{3}= \pm 0.005$, ± 0.010, ± 0.015, ± 0.020, ± 0.030 (Fig.6b).

In Fig.7 the skeletal points (points of maximum value of $\sqrt{3}\tau$, $|\Pi_1|$, and Y_1 for chosen strain amplitude at steady loop) for the stress - plastic strain curves, the Π_1 curves and the Y_1 curves (for mentioned cyclic program) are shown. They are compared with curves for monotonic load (Experiment 1 - $\sqrt{3}\tau$, Π_1, Y_1) in Fig.8.

Experiment 4. Cyclic tension - compresion with following strain amplitudes $\varepsilon_x^p=\pm 0.005$, ± 0.010, ± 0.015, ± 0.020

Similar cyclic program as in Experiment 3 was repeated for tension - compresion. The specimen was cyclically loaded with gradually increasing plastic strain amplitude $\varepsilon_x^p= \pm 0.005 - \pm 0.020$ and than the amplitude $\varepsilon_x^p= \pm 0.005$ was applied. Every strain amplitude change took place after reaching the steady state cycle for the former amplitude value.

In Fig.9 are shown the stress-plastic strain curves (thick lines) and the Π_1 curves (thin lines) for increasing strain amplitudes $\varepsilon_x^p=\pm 0.005$, ± 0.010, ± 0.015, ± 0.020. The solid line denotes the first cycle for certain amplitude and the dashed one - the stabilized loop.

In Fig.10 there are compared the stress - plastic strain curves, the curves and the Π curves for strain amplitude $\varepsilon_x^p= \pm 0.005$ for virgin material (Fig.10a) and for material with history of growing plastic strain amplitudes $\varepsilon_x^p= \pm 0.005$, ± 0.010

± 0.015, ± 0.020 (Fig.10b).

In Fig.11 the skeletal points (points of maximum value of $|\sqrt{3}\tau|$, $|\Pi_1|$, and Y_1 for chosen strain amplitude at steady loop) for the stress - plastic strain curves, the Π_1 curves and the Y_1 curves (for mentioned cyclic program) are shown. They are compared with curves for monotonic load (Experiment 2 $-\sqrt{3}\tau$, Π_1, Y_1) in Fig.12.

Experiment 5. Plastic prestrain in torsion followed by cyclic torsion loading

The specimen was plastically prestrained in torsion up to $\gamma^p/\sqrt{3}=0.092$ and then cyclically loaded with plastic strain amplitude $\gamma^p/\sqrt{3}=\pm 0.005$. The stress - strain (thick line), Π_1 (thin line), and Y_1 cyclic curves are shown in Fig.13. Solid lines show the values during the first cycle and the dashed lines for stabilized loops.

Experiment 6. Plastic prestrain in tension followed by cyclic tension - compresion loading

The specimen was plastically prestrained in tension up to $\varepsilon_x^p \doteq 0.092$ and then cyclically loaded with plastic strain amplitude $\varepsilon_x^p = \pm 0.005$. The stress - strain (thick line), Π_1 (thin line), and Y_1 cyclic curves are shown in Fig.14. Solid lines show the values during the first cycle and the dashed lines for stabilized loops.

Experiment 7. Influence of plastic prestrain on the subsequent cyclic behaviour.

The specimen was first cyclically loaded in torsion with plastic strain amplitude $\gamma^p/\sqrt{3}=\pm 0.005$ up to steady loop. Than it was plastically prestrained up to $\gamma^p/\sqrt{3}=0.092$ followed by cyclic loading with plastic strain amplitude $\gamma^p/\sqrt{3}= \pm 0.005$ up to steady state. The stress - strain, Π_1 and Y_1 curves for virgin material

(Fig.15a) and material after plastic prestrain (Fig.15b) are shown in Fig.15. Solid lines show the values for the first cycle and the dashed lines - for the stabilized loops.

Experiment 8. Tension compresion and torsion alternating cyclic program

The specimen was cyclically loaded in tension - compresion with plastic strain amplitude $\gamma^p/\sqrt{3}=\pm 0.015$ up to stabilized loop. Than, the cyclic loading in torsion with plastic strain amplitude $\gamma^p/\sqrt{3}=\pm 0.015$ was applied, also up to steady state. This program was followed by cyclic plastic loading with following amplitudes:

$\gamma^p/\sqrt{3}= \pm 0.005$ in torsion,
$\varepsilon_x^p = \pm 0.005$ in tension - compresion and
$\gamma^p/\sqrt{3}= \pm 0.005$ in torsion.

The stress - strain, Π_1 and γ_1 curves for this program are shown in Fig.16a and Fig.16b. As before the solid lines show the values for the first cycle and the dashed lines - for the stabilized loops.

Experiment 9. Out of phase loading with gradually increasing effective strain values: 0.005, 0.010 and 0.015

The specimen was loaded in out of phase manner shown in Fig.17. At the begining the axial tension (or pure torsion) was applied up to chosen effective strain value (for instance $\varepsilon_x^p=0.005$). Than the ratio $\sqrt{3}\varepsilon_x^p/\gamma^p$ was changing but the effective strain value $\varepsilon_e=(\varepsilon_x^p+\gamma^2/3)^{0.5}$ was kept constant. Such a loading, which in this coordinates is represented by the circle (one circle - one cycle), was repeated up to steady state and then, the new effective strain value was applied. In Fig.18 the uniaxial tension stress values and pure torsion stress values are shown for following out of phase cycles.

Skeleton points for tension (maximal uniaxial tension stress in steady loop) and torsion (maximal torsion stress $\sqrt{3}\tau_{max}$ in steady

loop) for constant effective strain values: 0.005, 0.010 and 0.015 are shown in Fig.19. They are compared with monotonic load for tension (Fig.19a) and torsion (Fig.19b) and with skeleton points for cyclic tension - compresion plastic loading and cyclic torsion plastioic loading.

Experiment 10.Out of phase loading for following effective strain values: 0.005, 0.010 and 0.005

The specimen was loaded in out of phase manner with constant effective strains 0.005 up to steady state. Than, the new value of effective strains ($\varepsilon_e^p=0.010$) was applied up to new steady loop and so on. The uniaxial stress values and pure torsion stress values for following cycles of this history are shown in Fig.20.

Experiment 11.Alternating program of cyclic plastic loading: torsion, tension - compresion and out of phase

The specimen was cyclically loaded in torsion with plastic strain amplitude $\gamma^p/\sqrt{3}=\pm 0.005$ up to steady state. Than the load was changed to cyclic tension - compresion with strain amplitude $\varepsilon_x^p=\pm 0.005$ followed by:

out of phase cycling for $\varepsilon_e^p=0.005$
out of phase cycling for $\varepsilon_e^p=0.010$
out of phase cycling for $\varepsilon_e^p=0.005$

Than the tension - compresion cyclic loading with plastic strain amplitude $\varepsilon_x^p=\pm 0.005$ was applied followed by torsion cyclic loading with strain amplitude $\gamma^p/\sqrt{3}=\pm 0.005$. Every strain amplitude change took place after reaching the steady state cycle for former amplitude value. The stress - strain, Π_1 and Y_1 curves for tension - compresion cyclic loading with plastic strain amplitude $\varepsilon_x^p=\pm 0.005$ just before out of phase loading program and after this program are shown in Fig.21. Solid lines show the values for the first cycle for chosen amplitude, and dashed lines - for stabilized loops.

Experiment 12. Alternating program of cyclic plastic loading: tension - compresion, torsion and out of phase

The specimen was cyclically loaded in tension - compresion with plastic strain amplitude $\varepsilon_x^p = \pm 0.005$ up to steady state. Than the load was changed to cyclic torsion with strain amplitude $\gamma^p/\sqrt{3} = \pm 0.005$ followed by out of phase cycling for $\varepsilon_e^p = 0.010$. Than, the torsion cyclic loading with plastic strain amplitude $\gamma^p/\sqrt{3} = \pm 0.005$ was applied followed by tension - compresion cyclic loading with strain amplitude $\varepsilon_x^p = \pm 0.005$. Every strain amplitude change took place after reaching the steady state cycle for former amplitude value. The stress - strain, Π_1 (Fig.22a) and Y_1 (Fig.22b) curves for tension - compresion cyclic loading and torsion cyclic loading before and after out of phase loading program are shown in Fig.22. Solid lines show the values for the first cycle of chosen amplitude, and dashed lines for the stabilized loops.

Experiment 13. Monotonic torsion load after history of torsion cyclic plasticity with following amplitudes:
$\gamma^p/\sqrt{3} = \pm 0.005, \pm 0.010, \pm 0.015, \pm 0.020, \pm 0.030, \pm 0.005$

The specimen was cyclically loaded in torsion with mentioned above plastic strain amplitudes. Every amplitude change took place after reaching the steady state cycle for former amplitude value. Than, the monotonic torsion load was applied. The monotonic plastic strain curve, Π_1 and Y_1 curves are shown in Fig.23.

Experiment 14. Monotonic tension load after history of tension - compresion cyclic plasticity with following amplitudes: $\varepsilon_x^p = \pm 0.005, \pm 0.010, \pm 0.015, \pm 0.020, \pm 0.005$

In this experiment the similar program to that in Experiment 13 was performed. The specimen was cyclically loaded in tension - compresion with mentioned above plastic strain amplitudes. Than, the monotonic tension was applied. The monotonic plastic strain curve, Π_1 and γ_1 curves are shown in Fig.24.

4. Conclusions

The simple plastic shear, plastic torsion, cyclic plastic shear, cyclic plastic tension - torsion and out of phase tests of 18G2A steel were performed. The specimens were loaded monotonically and cyclically with constant effective strain rate under controlled amplitude of plastic strains at room temperature. Using the technique of succesive unloadings (presented in [12]), the standard physical quantities and the stress jumps corresponding to opposite directions of plastic straining were measured. For the Huber - Mises yield surface the obtained results enable to follow the evolution of kinematic and isotropic hardening for such programs. The obtained results shows new effects concerning the influence of strain history on cyclic plasticity. They are similar to that obtained for 21CrMoV57 steel [12] and can be used for verification of existing theoretical approaches.

Acknowledgment

This work was carried out while the author held the Alexander von Humboldt Fellowship in Germany. The generosity of the Foundation, hospitality and attention of prof. Th.Lehmann at the

Institute of Mechanics I at Ruhr University Bochum are gratefully acknowledged.

References

1. Z.Mroz,On generalized kinematic hardenig rule with memory of maximal prestress,J.Mech.Appl.,5,242-260,1981
2. J.Chaboche,Viscoplastic constitutive equations for the description of cyclic and anisotropic behaviour of metals, Bull. Acad. Polon. Sci.,25,1,39-47,1977
3. T.Lehmann,General frame for the definition of constitutive laws for large non - isothermic elastic - plastic and elastic - visco - plastic deformations,The Constitutive Law in Thermoplasticity,CISM,1984
4. B.Raniecki,Thermodynamic aspects of cyclic and monotone plasticity,The Constitutive Law in Thermoplasticity,CISM,1984
5. E.Shiratori,K.Ikegami,K.Kaneko,Subsequent yield surface determined in consideration of the Bauschinger effect, Foundations of Plasticity,ed.by A.Sawczuk,Nordhoff,477-490, 1973
6. A.Philips,J.Tang,M.Ricciuti,Some new observations on yield surfaces,Acta Mech.,20,23-39,1974.
7. W.Szczepinski and J.Miastkowski,An experimental study of the effect of the prestraining history in the yield surfaces of an alluminium alloy,J.Mech.Phys.Solids,16,153-162,1968
8. K.Ikegami,Experimental plasticity on the anisotropy of metals,Proceedings of the Euromech Colloquium,115,1979, ed.J.Boehler,1982
9. R.Marianovic and W.Szczepinski,On the effect of biaxial cyclic loading on the yield surface of M-63 brass,Acta Mech., 23,65-74,1975
10. J.Miastkowski,On the effect of the two-dimentional cyclic loading on the yield surface of an aluminium alloy, Bull. Acad. Polon. Sci.,26,5,221-229,1978

11. M.Sliwowski,Behaviour of stress-strain diagrams for cyclic loadings,Bull. Acad. Polon. Sci.,27,2,115-123,1979
12. Th.Lehmann,B.Raniecki,W.Trampczynski,The Bauschinger effect in cyclic plasticity,Arch.Mech.,37,6,643-659

FIGURE CAPTIONS

Fig 1. Theoretical basis of unloading technique.

Fig 2. Application of unloading technique for monotonic tension.

Fig 3. Stress-strain, Π_1 and Y_1 curves for monotonic torsion.

Fig 4. Stress-strain, Π_1 and Y_1 curves for monotonic tension.

Fig 5. Stress-strain and Π_1 - curves for cyclic torsion with increasing plastic strain amplitudes: $\gamma^p/\sqrt{3} = \pm 0.005$, ± 0.010, ± 0.015, ± 0.020, ± 0.030.
(solid lines - the first cycles, dashed lines - the stabilised cycles)

Fig 6. Stress-strain, Π_1 and Y_1 curves for cyclic torsion with plastic strain amplitude
a) for virgin material
b) for material with history of increasing plastic strain amplitudes: $\gamma^p/\sqrt{3} = \pm 0.005 - \pm 0.030$
(solid lines - the first cycles, dashed lines - the stabilised cycles)

Fig 7. Skeleton curves for stress ($\sqrt{3}\tau_s$), Π_1 (Π_s) and Y_1 (Y_s) values for cyclic torsion in the case of increasing plastic strain amplitudes ($\gamma^p/\sqrt{3} = \pm 0.005 - \pm 0.030$) and skeleton points after decreasing the strain amplitude to $\gamma^p/\sqrt{3} = \pm 0.005$.

Fig 8. Comparison between the stress-strain, Π and curves for monotonic torsion and the skeleton points for stress ($\sqrt{3}\tau_s$), Π_1 (Π_s) and γ_1 (γ_s) for cyclic torsion in the case of increasing plastic strain amplitudes ($\gamma^p/\sqrt{3}=\pm 0.005$, ± 0.010, ± 0.015, ± 0.020, ± 0.030).

Fig 9. Stress-strain and Π_1 - curves for cyclic tension-compresion with increasing plastic strain amplitudes: $\varepsilon_x^p= \pm 0.005$, ± 0.010, ± 0.015, ± 0.020).
(solid lines - the first cycles, dashed lines - the stabilised cycles)

Fig 10. Stress-strain, Π_1 and γ_1 curves for cyclic tension-compresion with plastic strain amplitude $\varepsilon_x^p= \pm 0.005$
a) for virgin material
b) for material with history of increasing plastic strain amplitudes:
(solid lines - the first cycles, dashed lines - the stabilised cycles)

Fig 11. Skeleton curves for stress (σ_s), Π_1 (Π_s) and γ_1 (γ_s) values for cyclic tension-compresion in the case of increasing plastic strain amplitudes ($\varepsilon_x^p= \pm 0.005 - \pm 0.020$) and skeleton points after decreasing the strain amplitude to $\varepsilon_x^p= \pm 0.005$

Fig 12. Comparison between the stress-strain, Π_1 and γ_1 curves for monotonic tension and the skeleton points for stress (σ_s), Π_1 (Π_s) and γ_1 (γ_s) for cyclic tension-compresion in the case of increasing plastic strain amplitudes ($\varepsilon_x^p=\pm 0.005 - \pm 0.020$)

Fig 13. Stress-strain, Π_1 and Y_1 cyclic torsion curves for plastic strain amplitude $\gamma^p/\sqrt{3} = \pm 0.005$ after plastic torsion prestrain $\gamma^p/\sqrt{3} = 0.092$.
(solid lines - the first cycles, dashed lines - the stabilised cycles)

Fig 14. Stress-strain, Π_1 and γ_1 cyclic tension-compresion curves for plastic strain amplitude $\varepsilon_x^p = \pm 0.005$ after plastic tension prestrain $\varepsilon_x^p = 0.092$.
(solid lines - the first cycles, dashed lines - the stabilised cycles)

Fig 15. Stress-strain, Π_1 and γ_1 curves for cyclic torsion with plastic strain amplitude $\gamma^p/\sqrt{3} = \pm 0.005$
a) for virgin material
b) for material after plastic torsion prestrain $\gamma^p/\sqrt{3} = 0.092$
(solid lines - the first cycles, dashed lines - the stabilised cycles)

Fig 16. Stress-strain, Π_1 (Fig.16a) and Y_1 (Fig.16b) curves for following cyclic program:

tension-compresion with plastic strain amplitude $\varepsilon_x^p = \pm 0.015$
reverse torsion with plastic strain amplitude $\gamma^p/\sqrt{3} = \pm 0.015$
reverse torsion with plastic strain amplitude $\gamma^p/\sqrt{3} = \pm 0.005$
tension-compresion with plastic strain amplitude $\varepsilon_x^p = \pm 0.005$
reverse torsion with plastic strain amplitude $\gamma^p/\sqrt{3} = \pm 0.005$

(solid lines - the first cycles, dashed lines - the stabilised cycles)

Fig 17. The out of phase loading (one circle = one cycle)

Fig 18. Maximum stress values (σ_{max} , $\sqrt{3}\tau_{max}$) as a function of cycle number in the case of out of phase loading with gradually increasing effective strain values: ε_e^p =0.005, 0.010 and 0.015.

Fig 19. Comparison between the stress-strain curves for monotonic tension (Fig.19a) (torsion-Fig.19b) and the skeleton points for stress in the case of tension-compresion cyclic loading (Fig.19a) (cyclic torsion-Fig.19b), and the out of phase skeleton points.

Fig 20. Maximum stress values (σ_{max} , $\sqrt{3}\tau_{max}$) as a function of cycle number in the case of out of phase loading for following effective strain values: ε_e^p =0.005,0.010 and 0.005.

Fig 21. Stress-strain, Π_1 and γ_1 curves for cyclic tension-compresion with plastic strain amplitude

a) for virgin material

b) for material after out of phase cyclic loading with following strain amplitudes: ε_e^p =0.005, 0.010, 0.005.

(solid lines - the first cycles, dashed lines - the stabilised cycles)

Fig 22.Stress-strain, Π_1 (Fig.22a) and Υ_1 (Fig.22b) cyclic curves

Fig.22a/1 -tension-compresion with plastic strain amplitude

Fig.22b/1 $\varepsilon_x^p = \pm 0.005$ followed by cyclic torsion with plastic strain amplitude $\gamma^p/\sqrt{3} = \pm 0.005$

Fig.22a/2 -cyclic torsion with plastic strain amplitude

Fig.22b/2 $\gamma^p/\sqrt{3} = \pm 0.005$ followed by cyclic tension-compresion with plastic strain amplitude $\varepsilon_x^p = \pm 0.005$ for material after out of phase cycling with constant effective strain $\varepsilon_e^p = 0.010$.

(solid lines - the first cycles, dashed lines - the stabilised cycles)

Fig 23.Stress-strain, Π_1 and Υ_1 curves for monotonic torsion after torsion cyclic program for following plastic strain amplitudes: $\gamma^p/\sqrt{3} = \pm 0.005$, ± 0.010, ± 0.015, ± 0.020, ± 0.030, ± 0.005.

Fig 24.Stress-strain, Π_1 and Υ_1 curves for monotonic tension after tension - compresion cyclic program for following plastic strain amplitudes: $\varepsilon_x^p = \pm 0.005$, ± 0.010, ± 0.015, ± 0.020, ± 0.005.

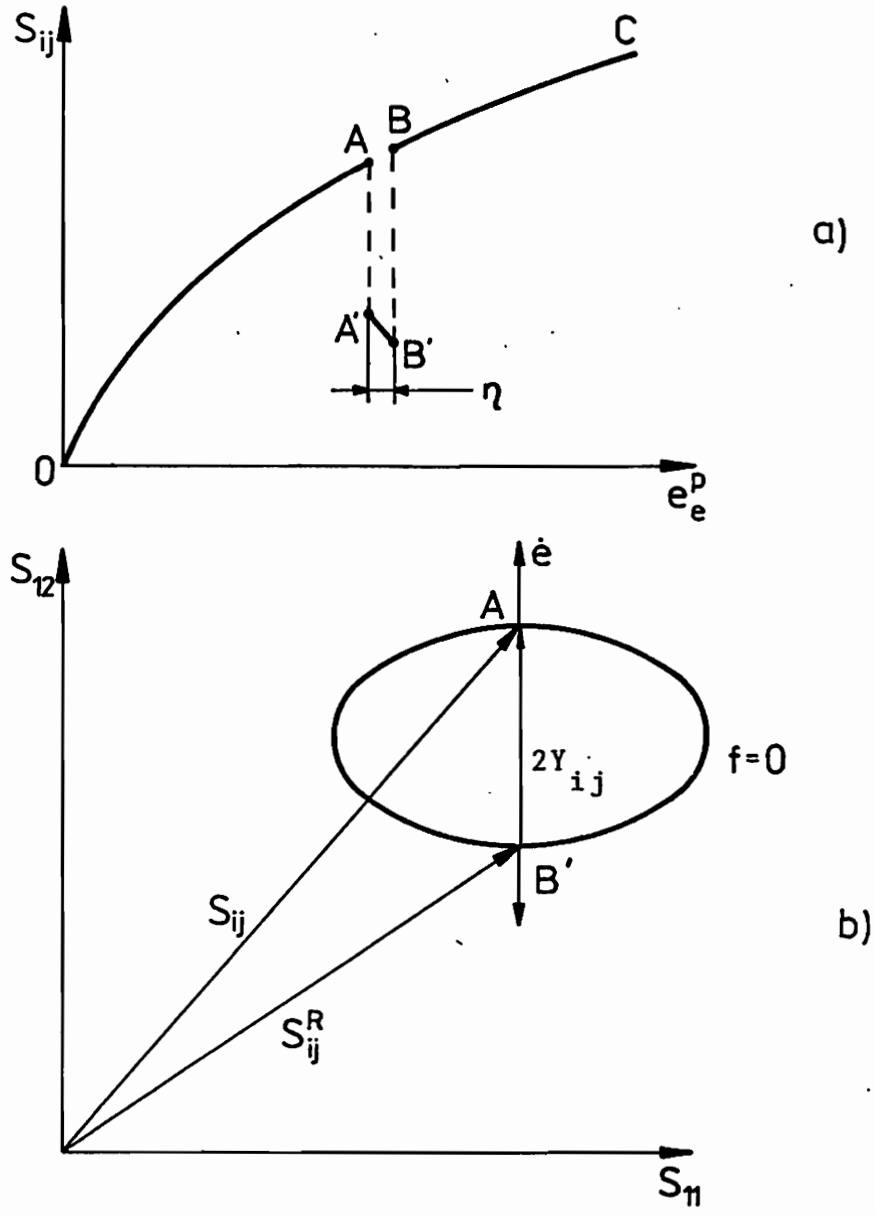

Fig.1

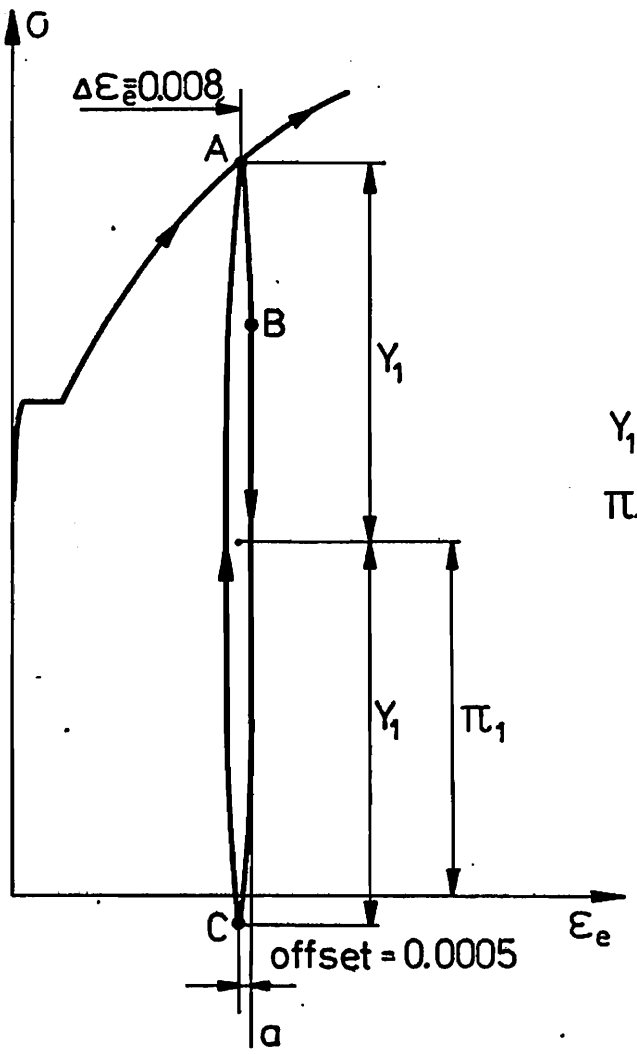

Fig.2

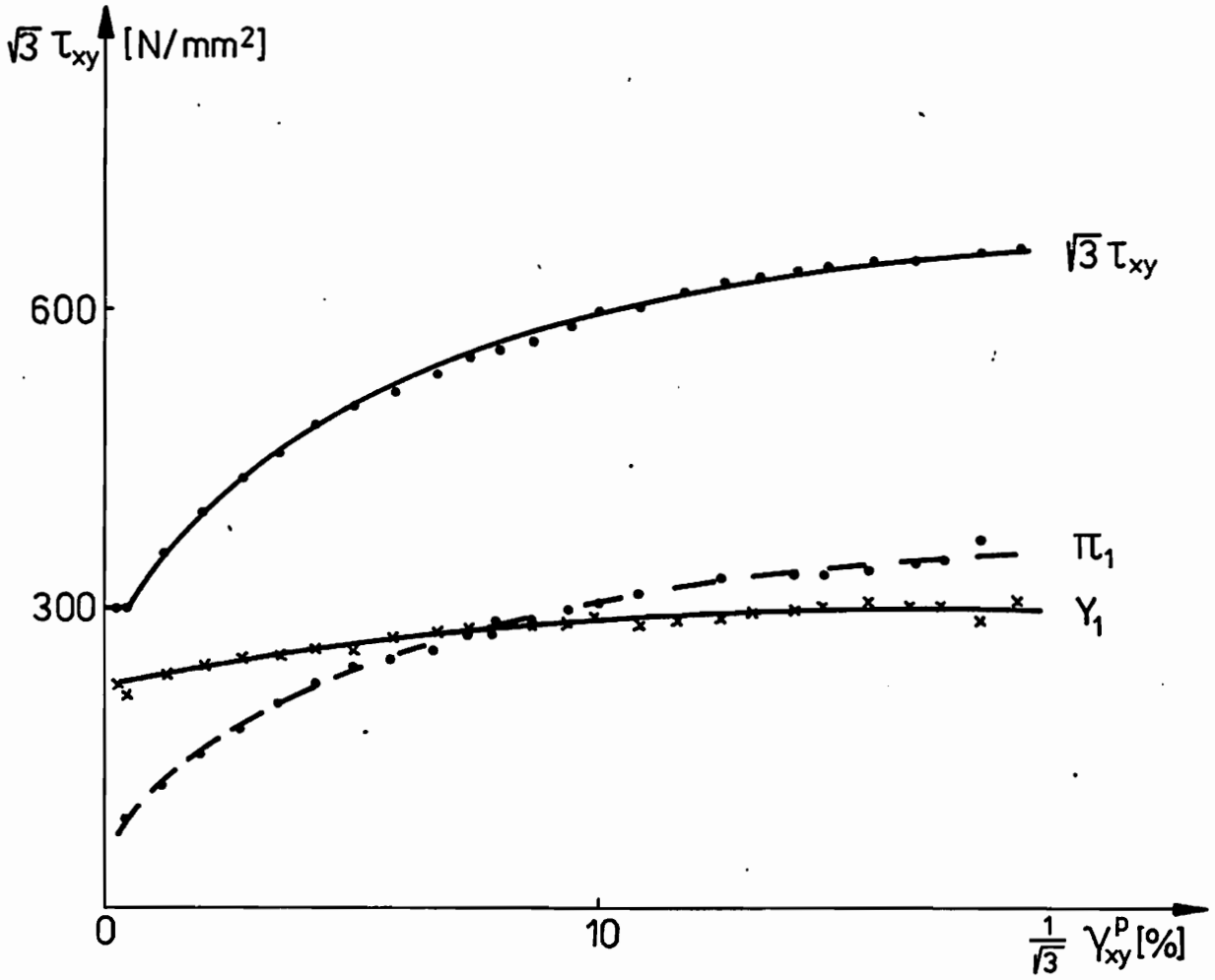

Fig. 3

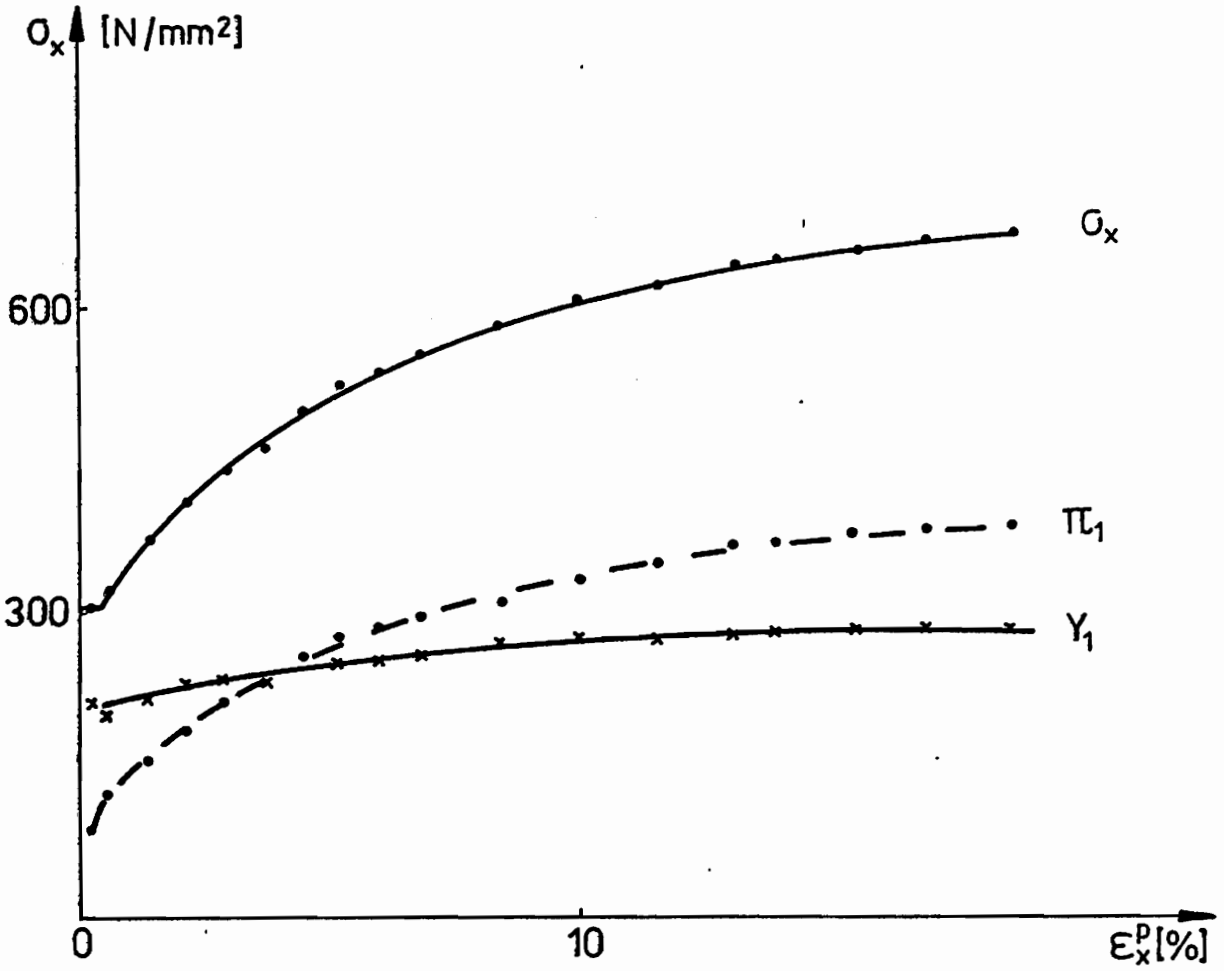

Fig.4

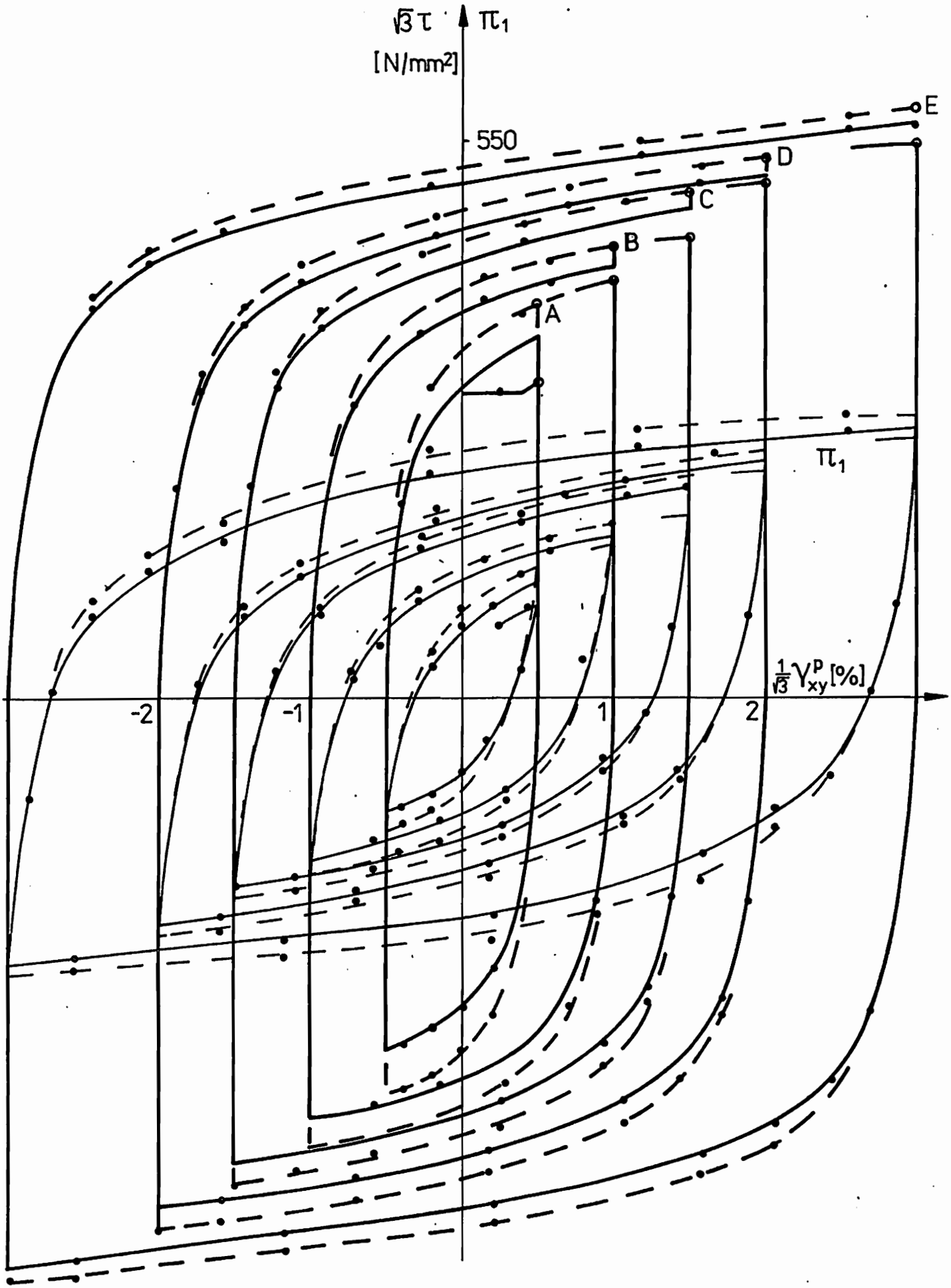

Fig.5

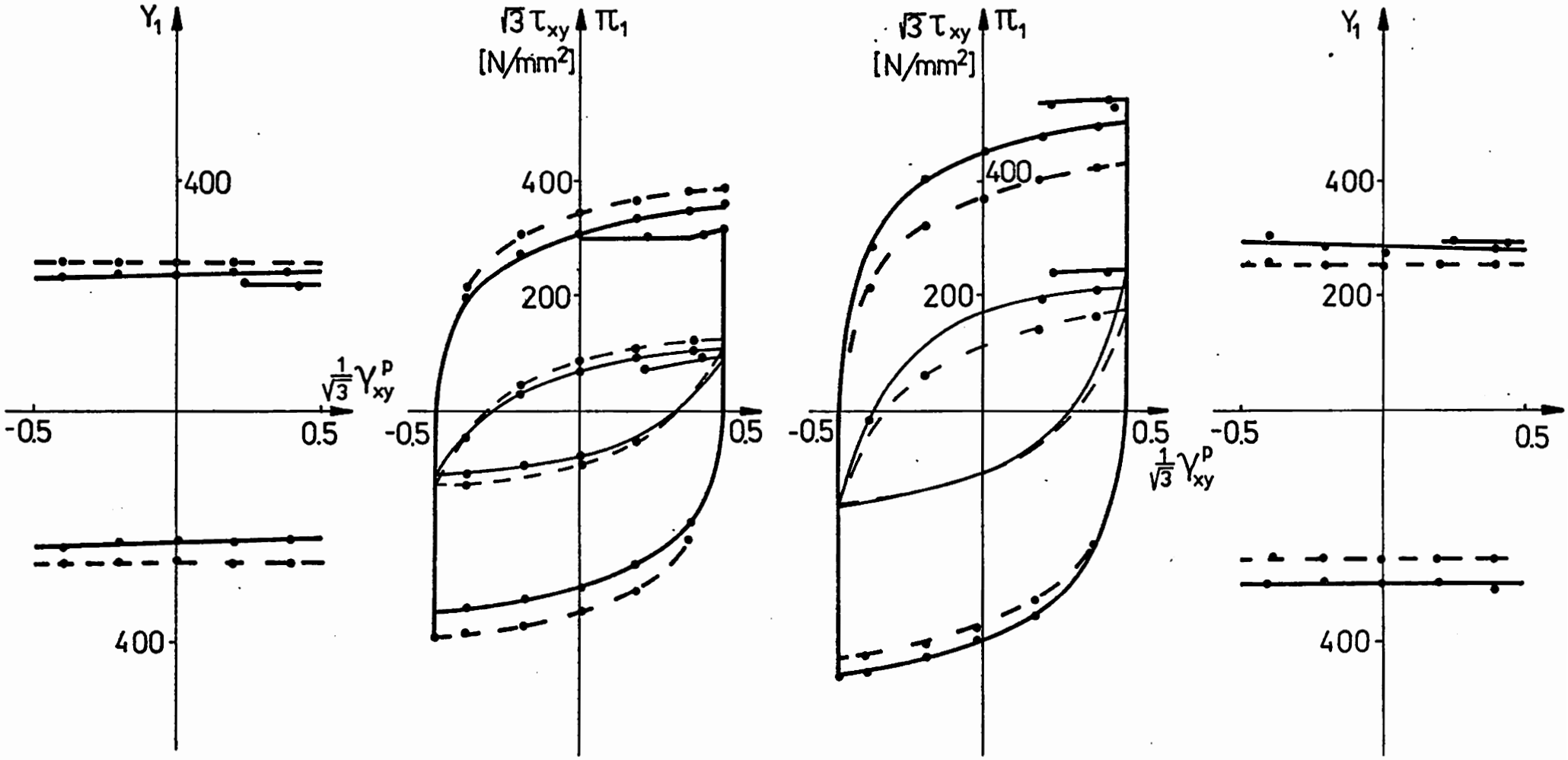
Y1
400
400
-0.5
0.5
1/√3 γxy^p
√3 τxy [N/mm²]
τ1
400
200
-0.5
0.5
a)
√3 τxy [N/mm²]
τ1
400
200
-0.5
0.5
1/√3 γxy^p
Y1
400
200
400
-0.5
0.5
b)

Fig.6

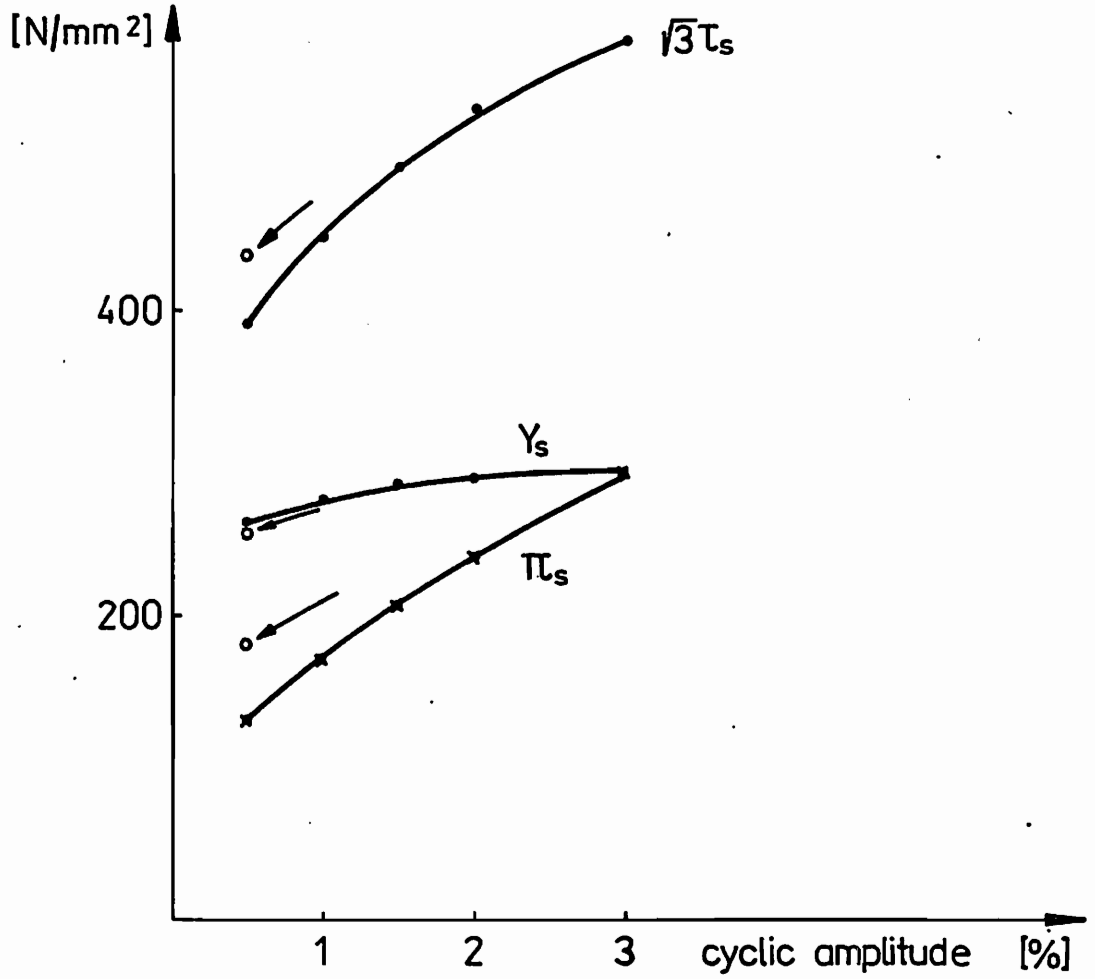

Fig. 7

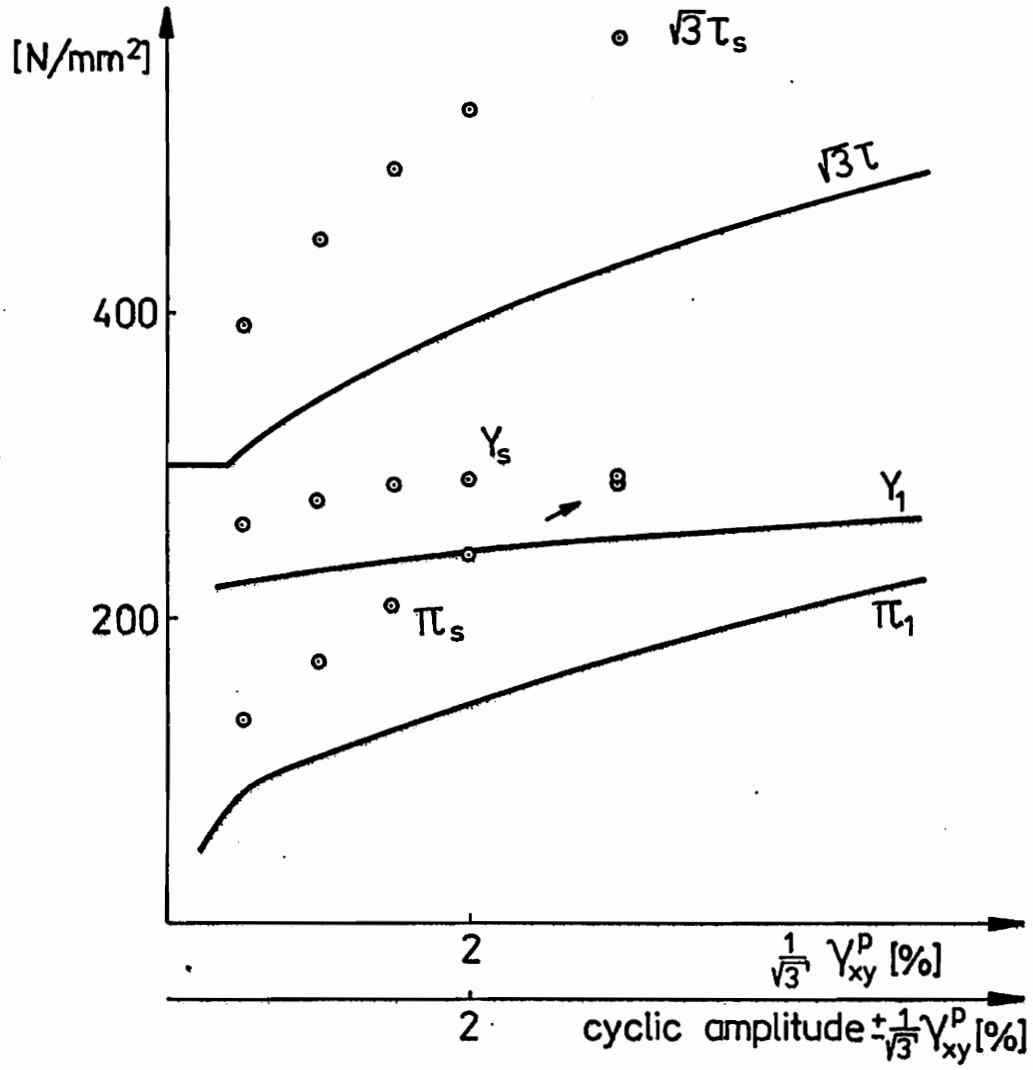
[N/mm²]
√3τs
√3τ
400
Ys
8
Y1
200
πs
π1
2
1/√3 γxy^p [%]
2
cyclic amplitude ±1/√3 γxy^p [%]

Fig. 8

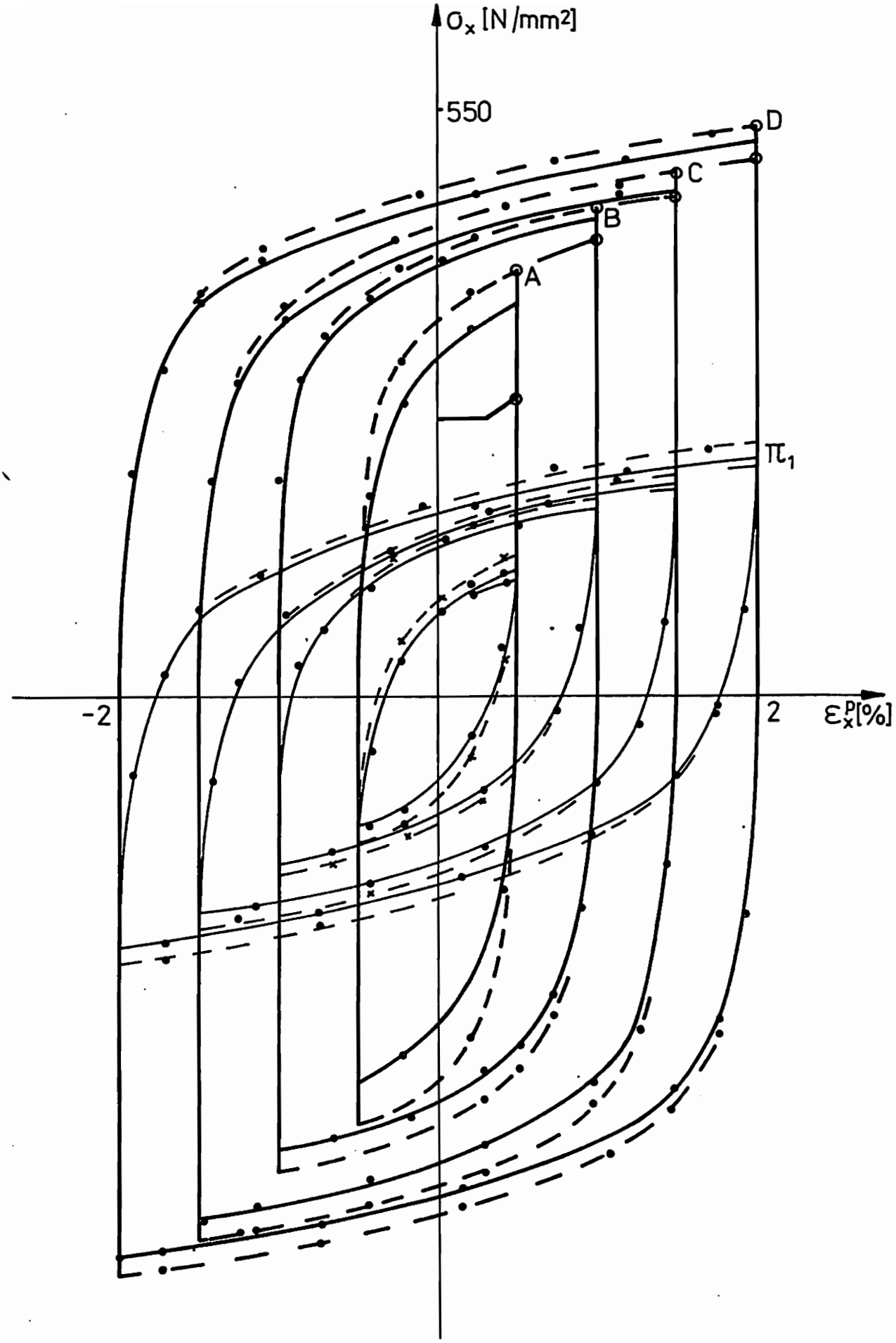

Fig.9

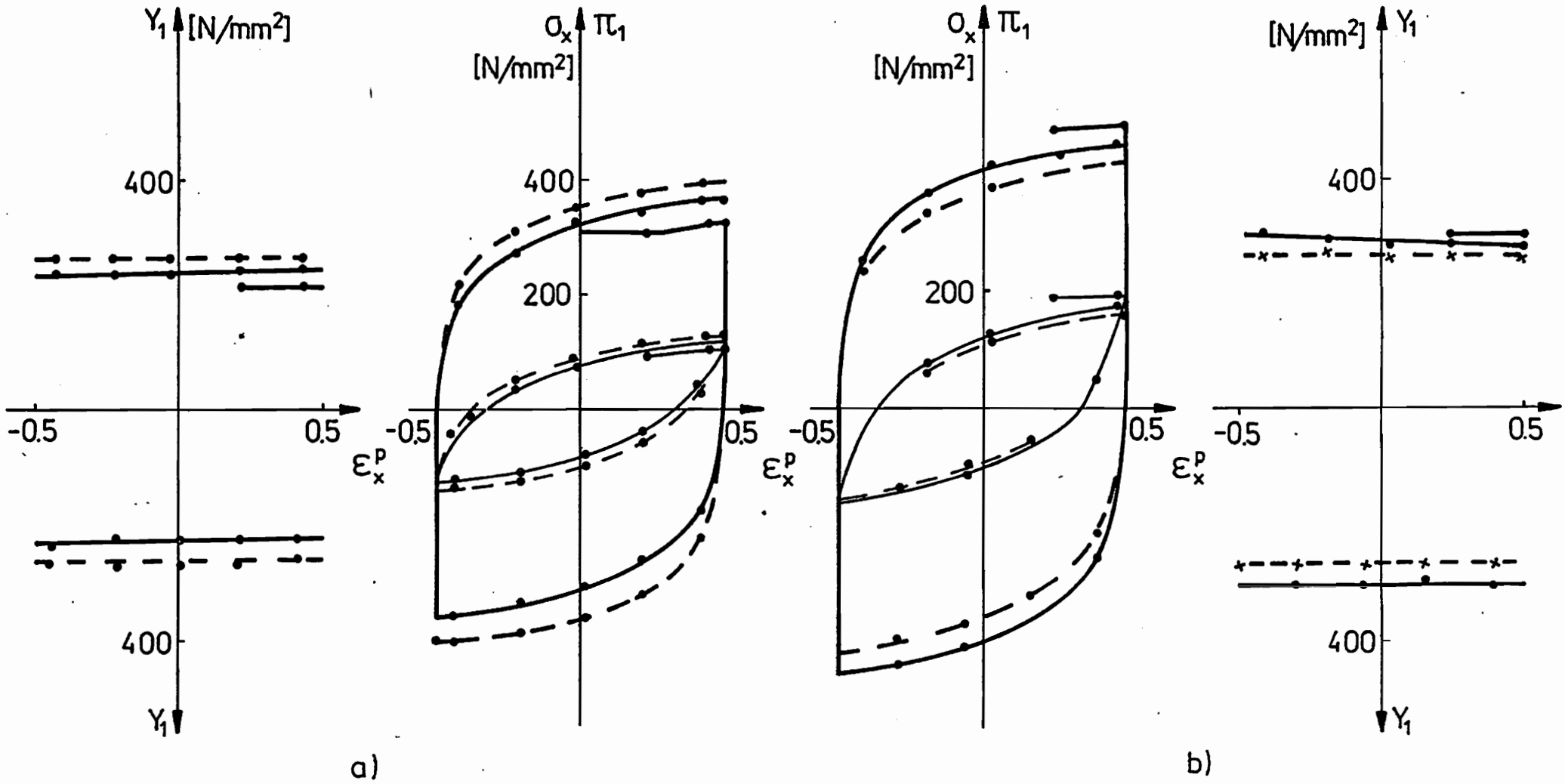
Y_1 [N/mm²]
400
-0.5
0.5
400
Y_1
a)
σ_x τ_1
[N/mm²]
400
200
-0.5
0.5
ε_x^p
σ_x τ_1
[N/mm²]
200
-0.5
0.5
ε_x^p
[N/mm²] Y_1
400
-0.5
0.5
400
Y_1
b)

Fig.10

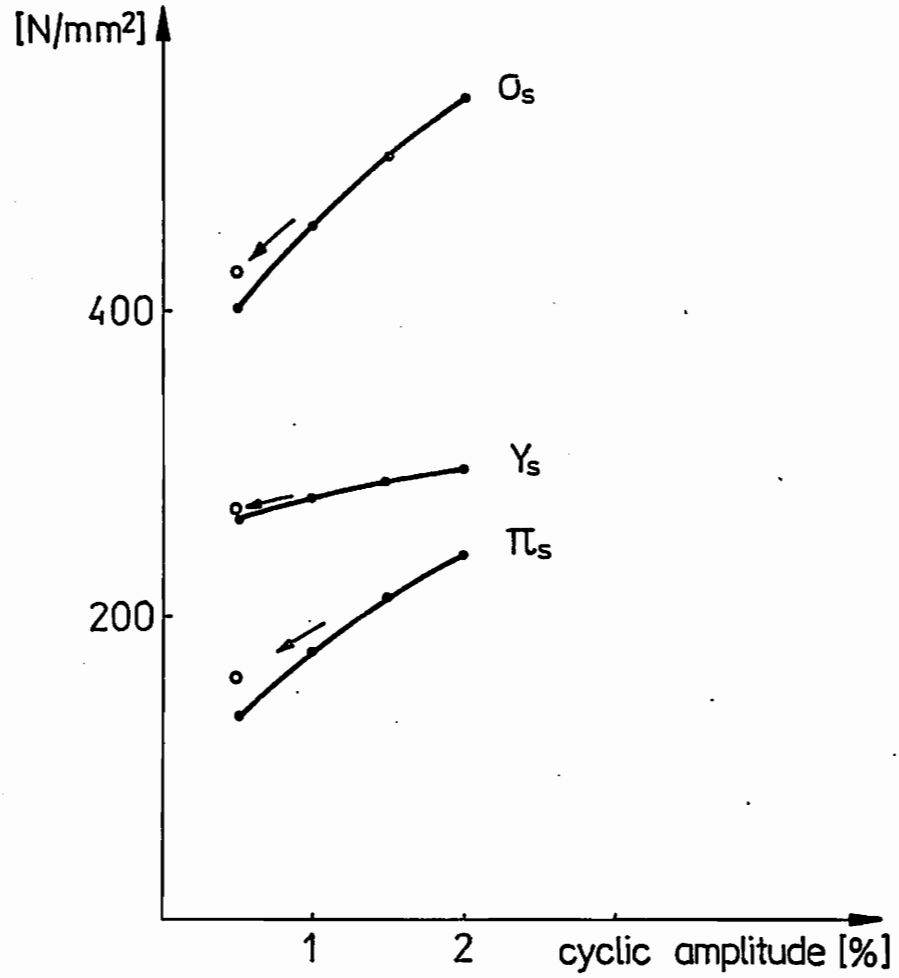

Fig. 11

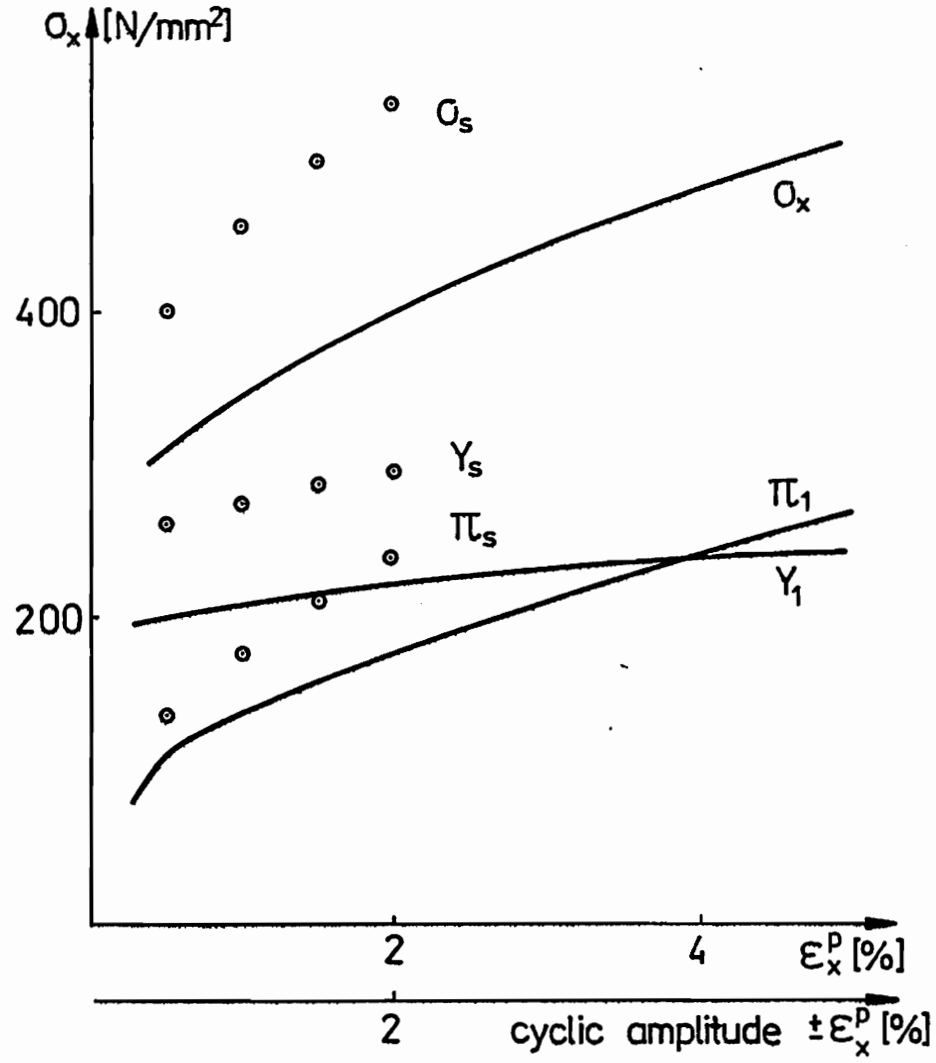
σ_x [N/mm²]
σ_s
σ_x
400
Y_s
π_1
π_s
Y_1
200
2
4
ε_x^p [%]
2
cyclic amplitude $\pm\varepsilon_x^p$ [%]

Fig. 12

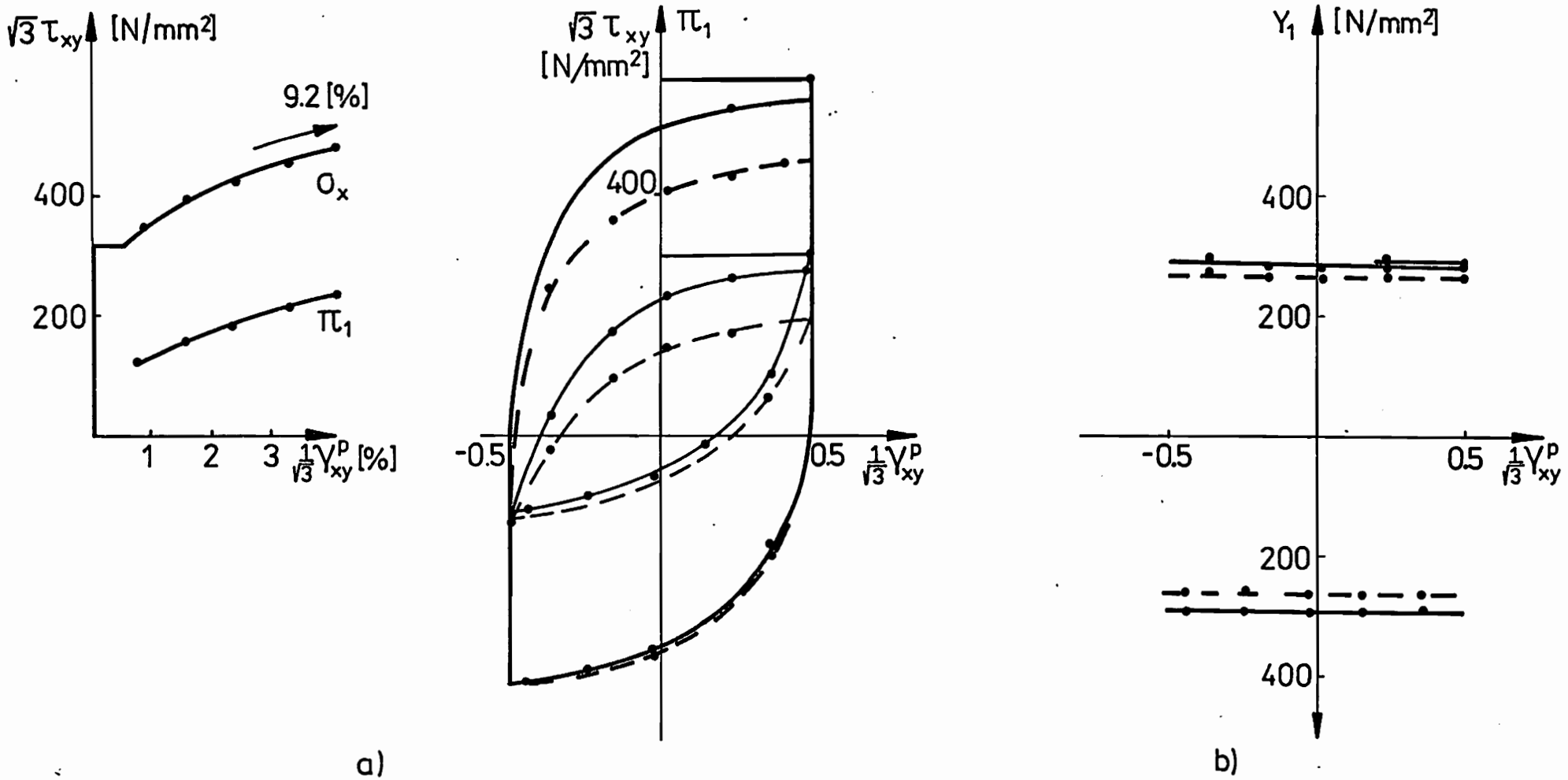
√3 τxy [N/mm²]
9.2 [%]
400
200
σx
πτ1
1
2
3
1/√3 γ^p_xy [%]
a)
√3 τxy [N/mm²]
πτ1
400
-0.5
0.5
1/√3 γ^p_xy
Y1 [N/mm²]
400
200
-0.5
0.5
1/√3 γ^p_xy
200
400
b)

Fig.13

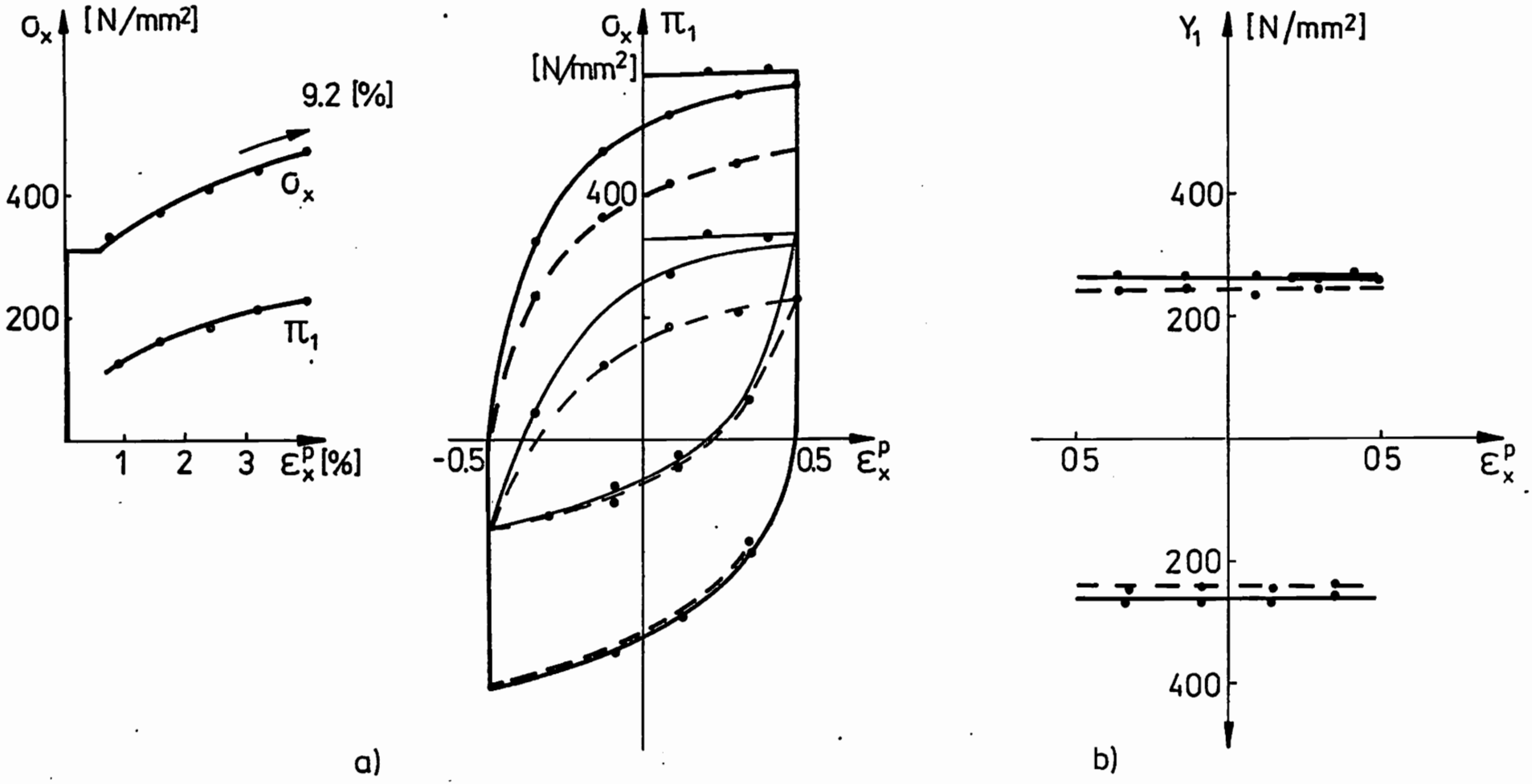
σx [N/mm2]
9.2 [%]
400
200
σx
π1
1 2 3 εxp [%]
a)
σx π1
[N/mm2]
400
-0.5
0.5 εxp
Y1 [N/mm2]
400
200
05
05 εxp
200
400
b)

Fig.14

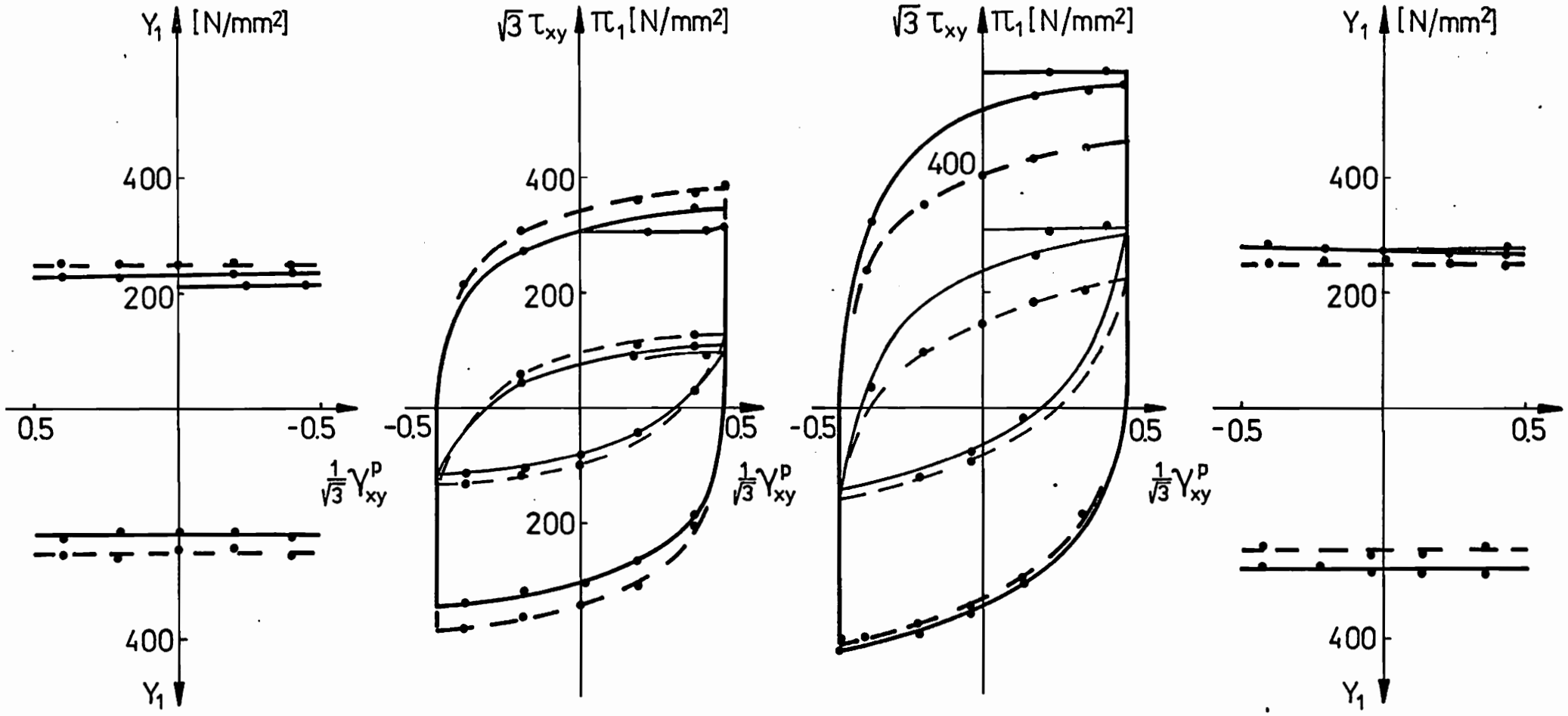
Y1 [N/mm2]
400
200
0.5
-0.5
1/√3 γ^p_xy
400
√3 τxy
τ1 [N/mm2]
400
200
-0.5
0.5
1/√3 γ^p_xy
200
400
Y1
a)
√3 τxy
τ1 [N/mm2]
400
-0.5
0.5
1/√3 γ^p_xy
Y1 [N/mm2]
400
200
-0.5
0.5
400
Y1
b)

Fig. 15

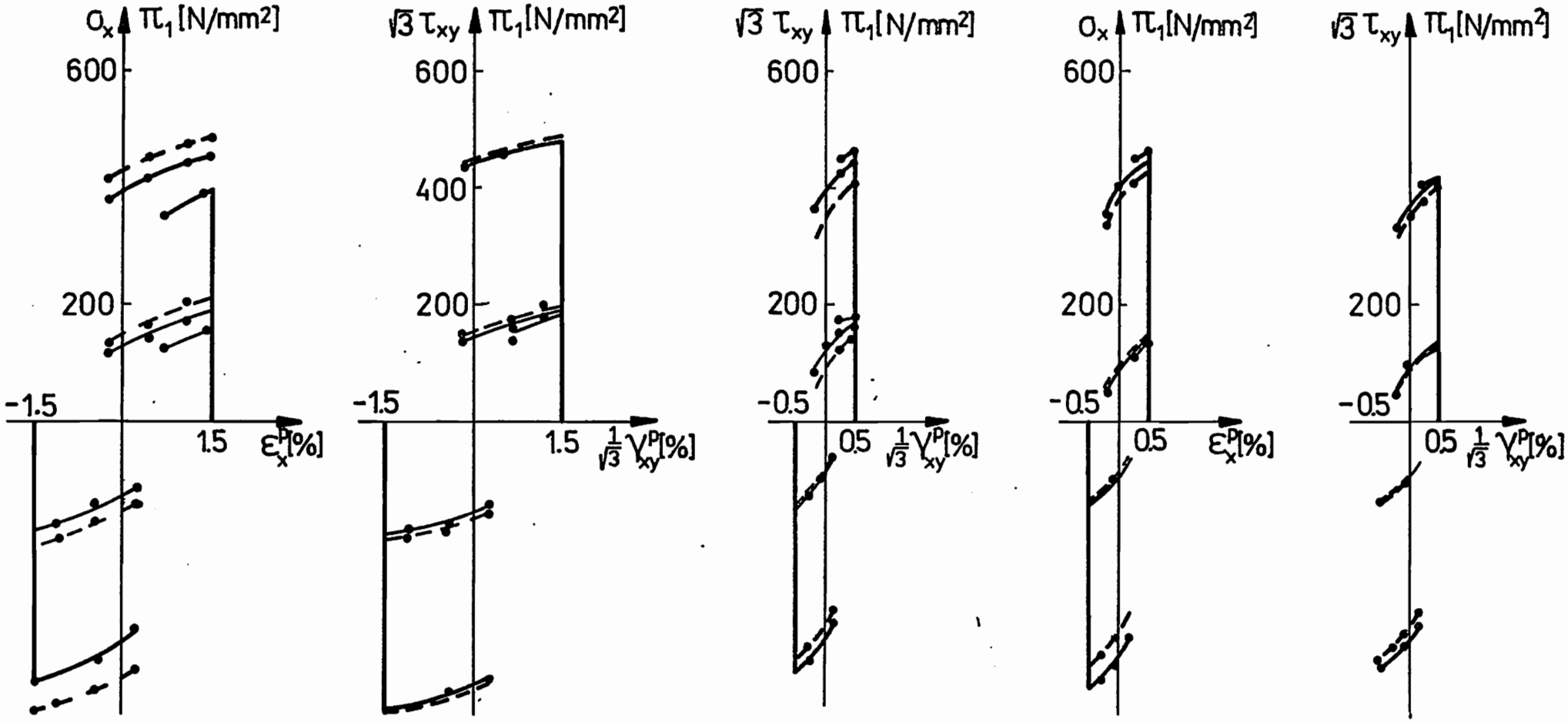
σx
τ1 [N/mm2]
600
200
-1.5
1.5
εxP[%]
√3 τxy
τ1[N/mm2]
600
400
200
-1.5
1.5
1/√3 γxyP[%]
√3 τxy
τ1[N/mm2]
600
200
-0.5
0.5
1/√3 γxyP[%]
σx
τ1[N/mm2]
600
200
-0.5
0.5
εxP[%]
√3 τxy
τ1[N/mm2]
200
-0.5
0.5
1/√3 γxyP[%]

Fig. 16.a

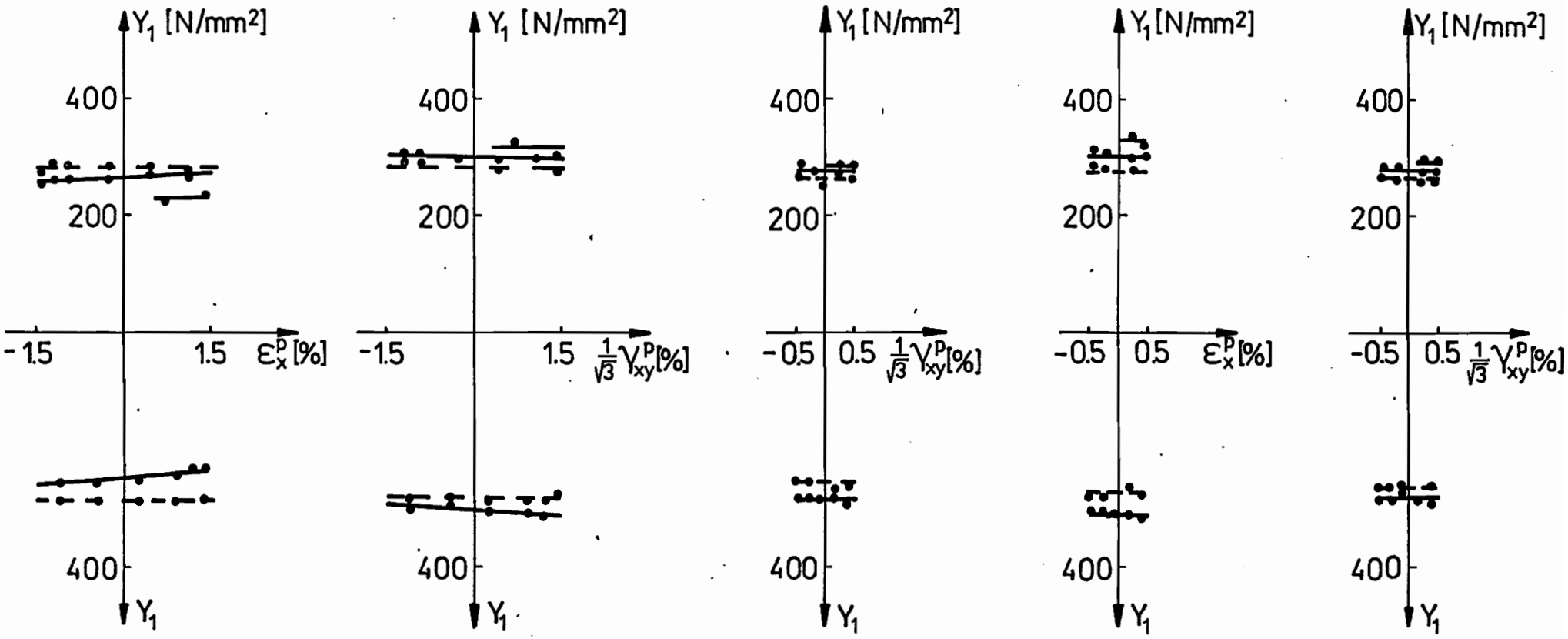
Y1 [N/mm2]
400
200
-1.5
1.5
ε_x^p [%]
400
Y1
Y1 [N/mm2]
400
200
-1.5
1.5
$\frac{1}{\sqrt{3}}\gamma_{xy}^p$ [%]
400
Y1
Y1 [N/mm2]
400
200
-0.5
0.5
$\frac{1}{\sqrt{3}}\gamma_{xy}^p$ [%]
400
Y1
Y1 [N/mm2]
400
200
-0.5
0.5
ε_x^p [%]
400
Y1
Y1 [N/mm2]
400
200
-0.5
0.5
$\frac{1}{\sqrt{3}}\gamma_{xy}^p$ [%]
400
Y1

Fig.16.b

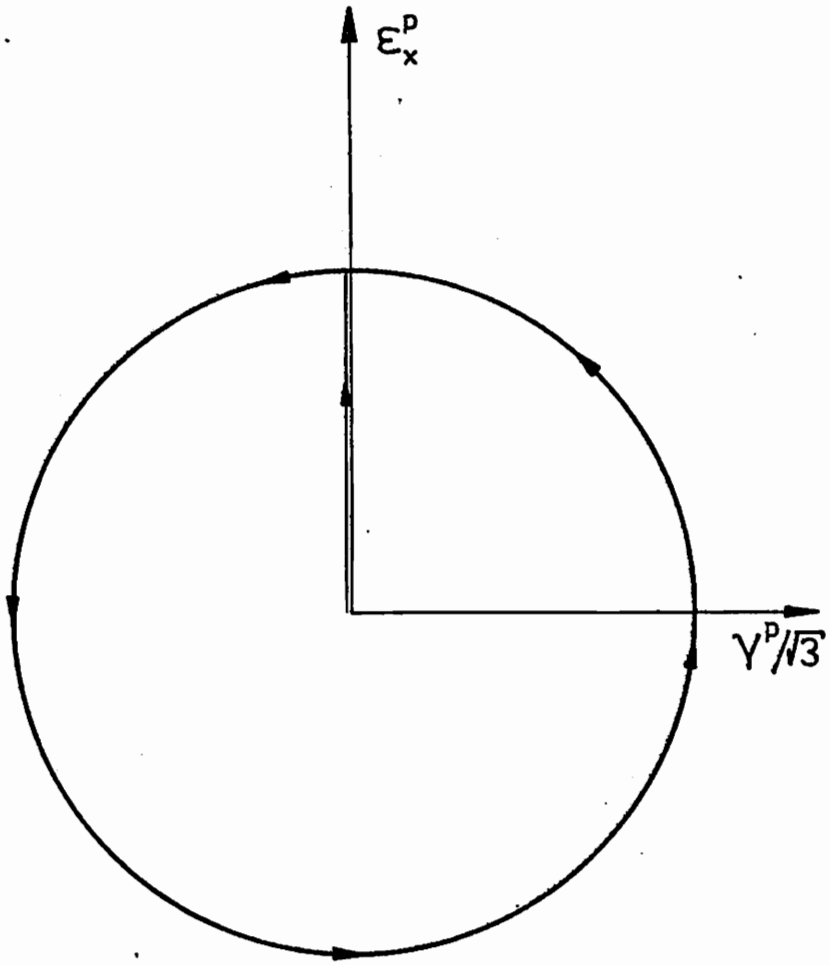

Fig. 17

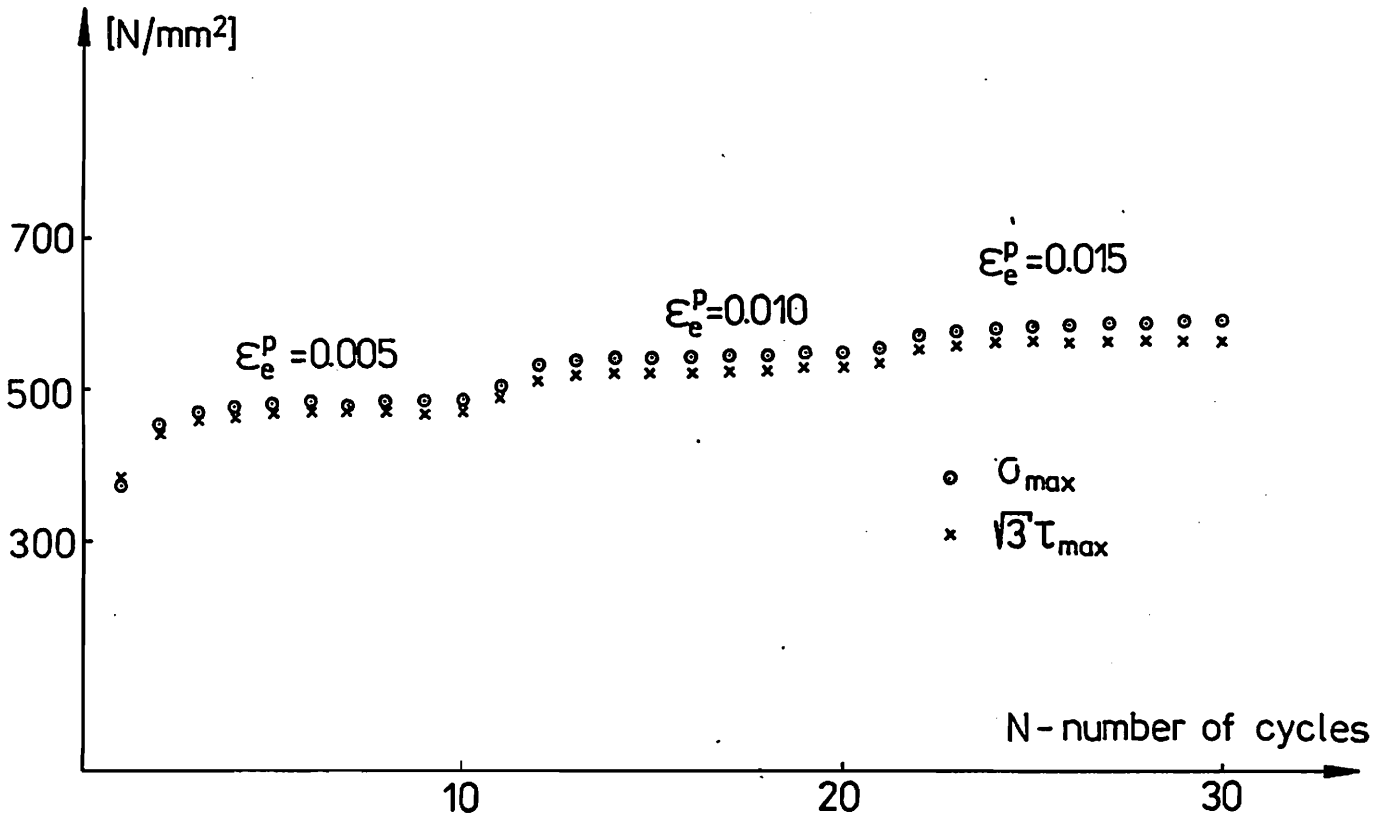
[N/mm2]
700
500
300
ε_e^p=0.005
ε_e^p=0.010
ε_e^p=0.015
σ_{max}
$\sqrt{3}\tau_{max}$
N - number of cycles
10
20
30

Fig. 18

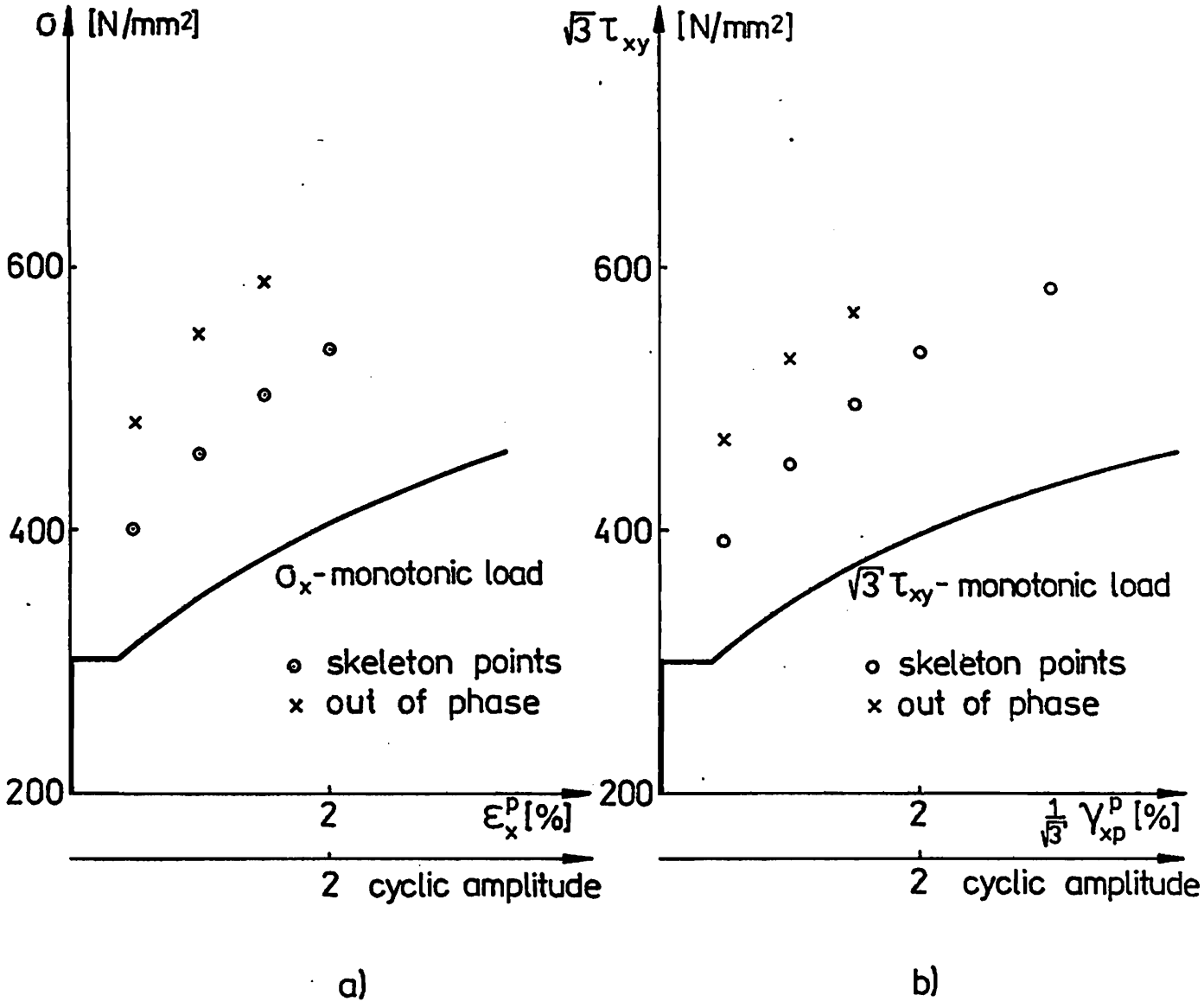
σ [N/mm2]
600
400
200
σx - monotonic load
skeleton points
out of phase
2
εxp [%]
2 cyclic amplitude
a)
√3 τxy [N/mm2]
600
400
200
√3 τxy - monotonic load
skeleton points
out of phase
2
1/√3 γxp [%]
2 cyclic amplitude
b)

Fig. 19

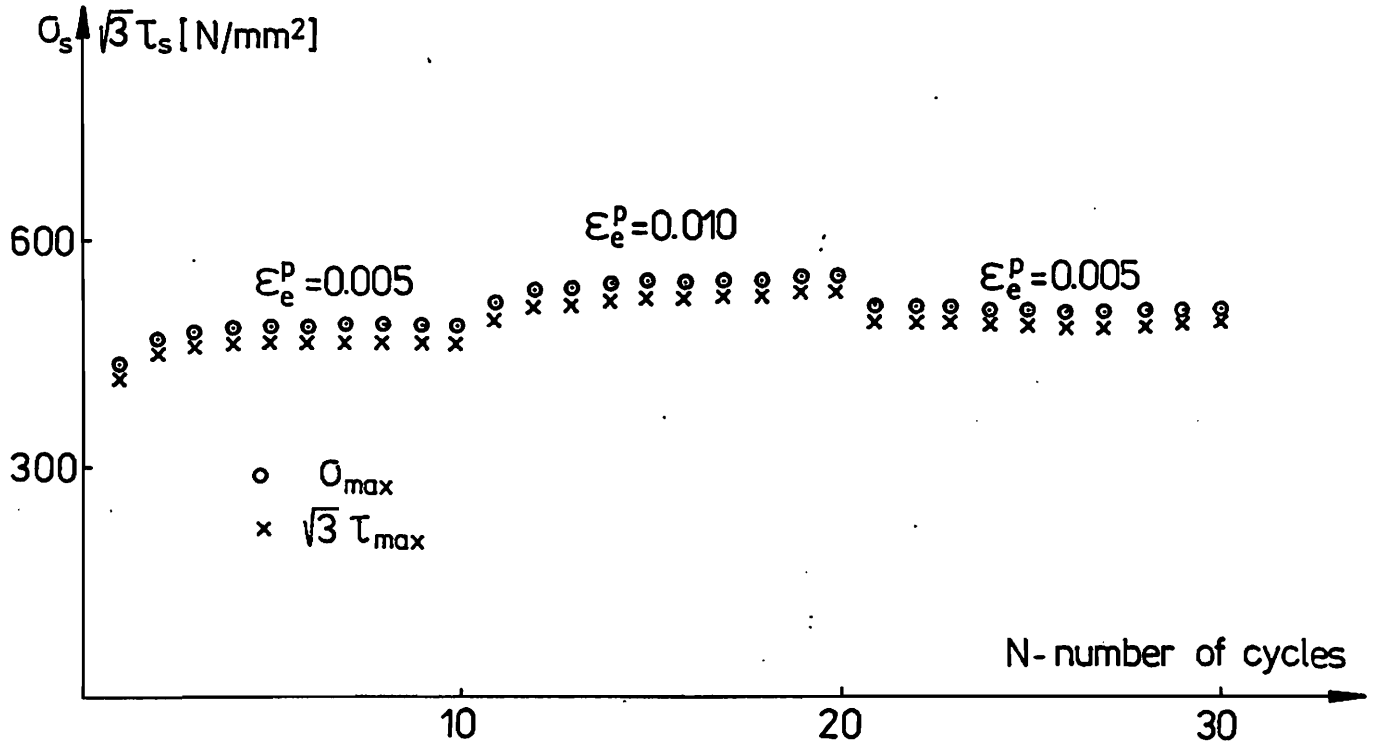
σ_s $\sqrt{3}\tau_s$ [N/mm²]
600
300
ε_e^p=0.010
ε_e^p=0.005
ε_e^p=0.005
σ_{max}
$\sqrt{3}\tau_{max}$
N - number of cycles
10
20
30

Fig.20

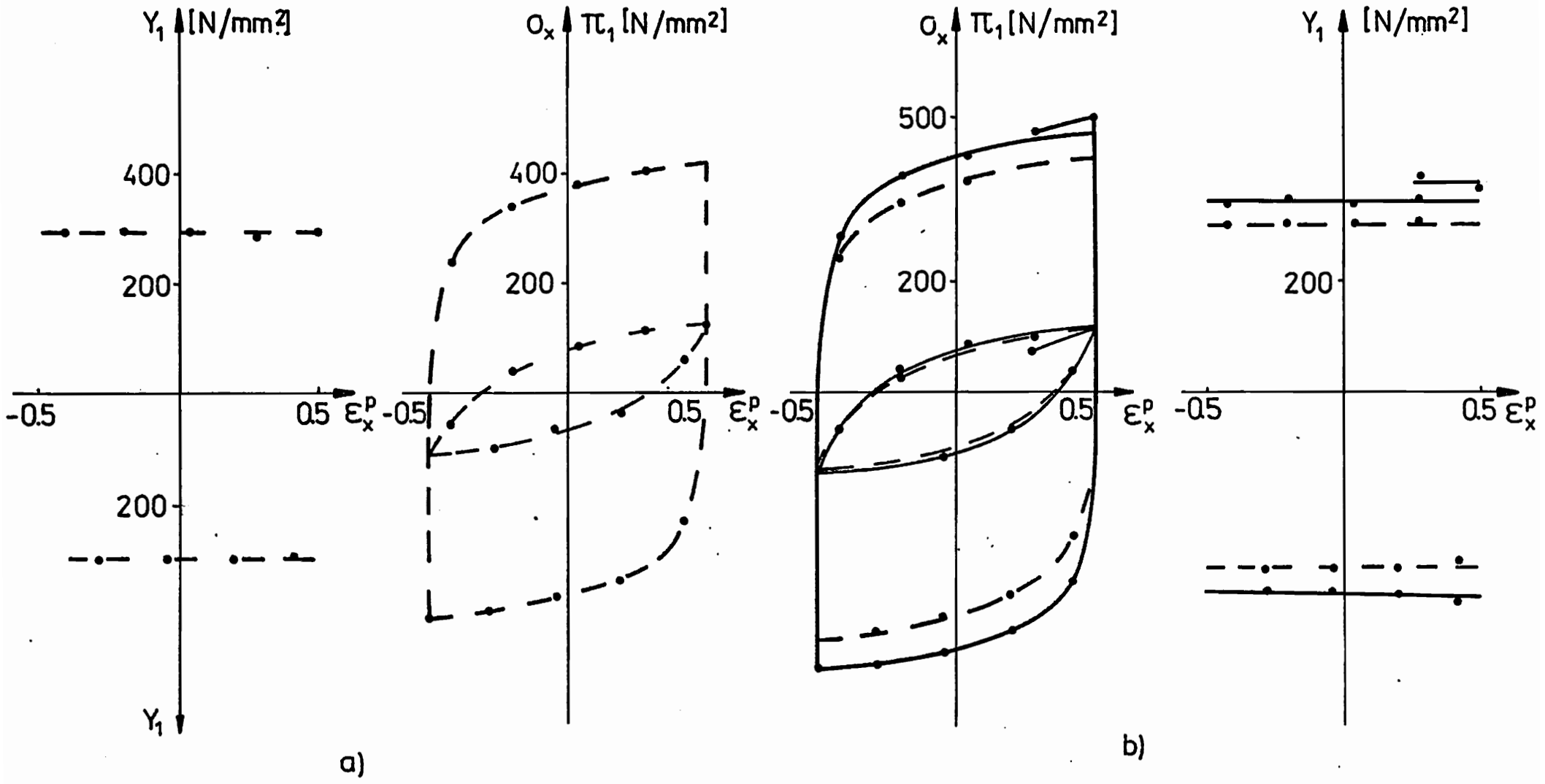
Y1 [N/mm2]
400
200
200
-0.5
0.5
εxp
Y1
a)
σx τ1 [N/mm2]
400
200
-0.5
0.5
εxp
σx τ1 [N/mm2]
500
200
-0.5
0.5
εxp
Y1 [N/mm2]
200
-0.5
0.5
εxp
b)

Fig. 21

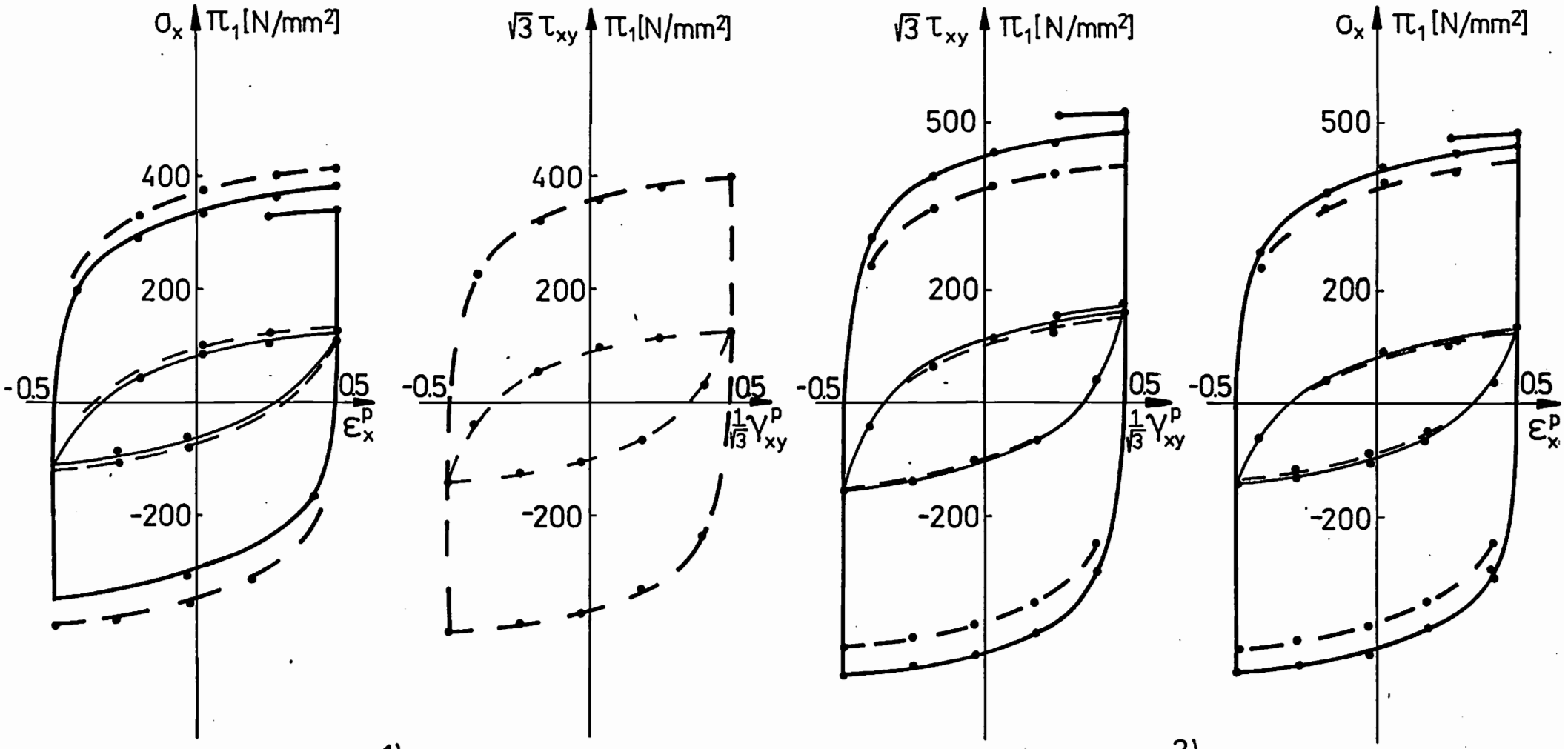
σx
τ1 [N/mm²]
400
200
-200
-0.5
0.5
εxp
1)
√3 τxy
τ1 [N/mm²]
400
200
-200
-0.5
0.5
1/√3 γxyp
√3 τxy
τ1 [N/mm²]
500
200
-200
-0.5
0.5
1/√3 γxyp
σx
τ1 [N/mm²]
500
200
-200
-0.5
0.5
εxp
2)

Fig. 22.a

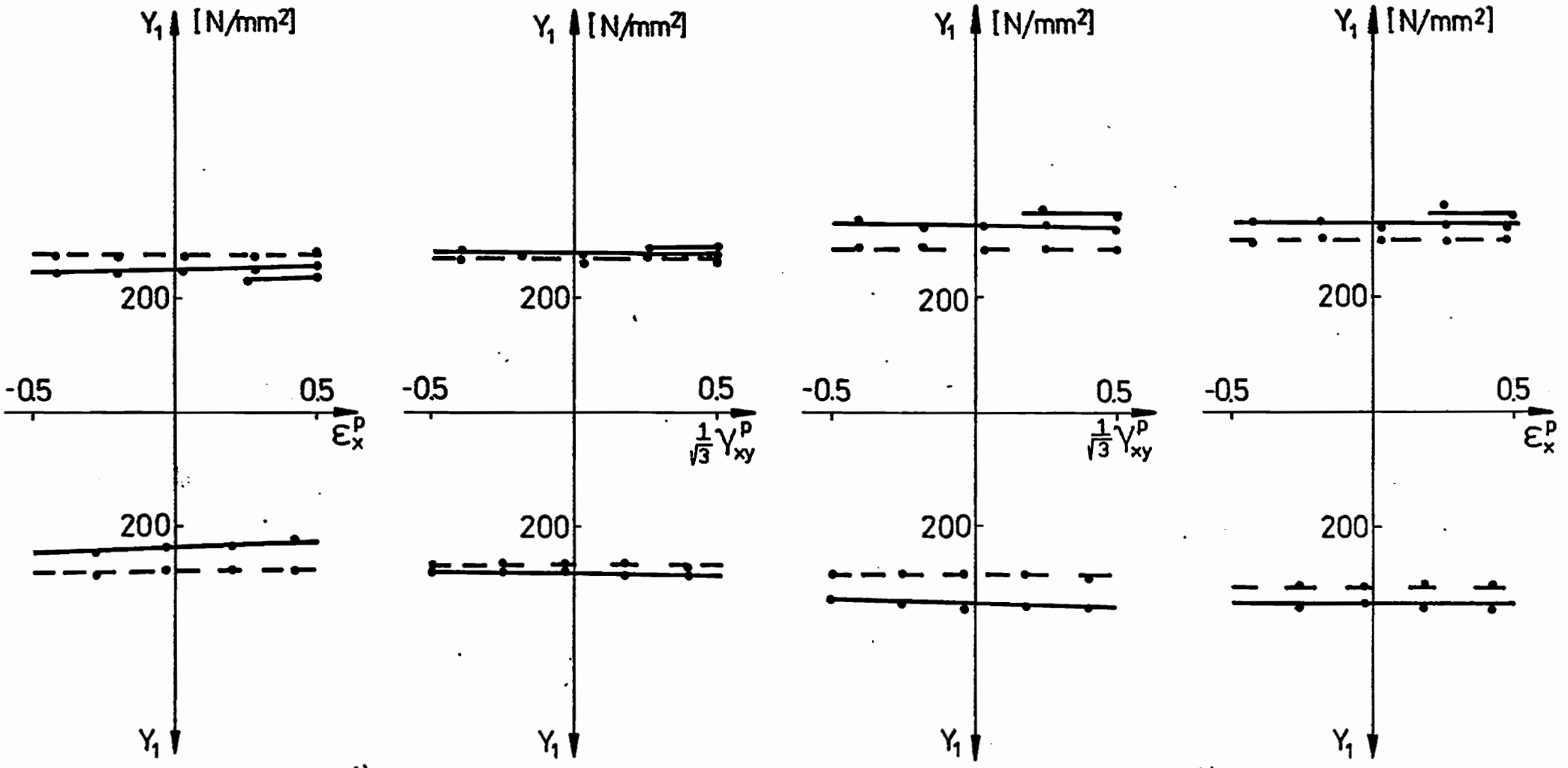
Y1 [N/mm2]
200
-0.5
0.5
εxp
Y1
1)
Y1 [N/mm2]
200
-0.5
0.5
1/√3 γxyp
Y1
Y1 [N/mm2]
200
-0.5
0.5
1/√3 γxyp
Y1
Y1 [N/mm2]
200
-0.5
0.5
εxp
Y1
2)

Fig.22.b

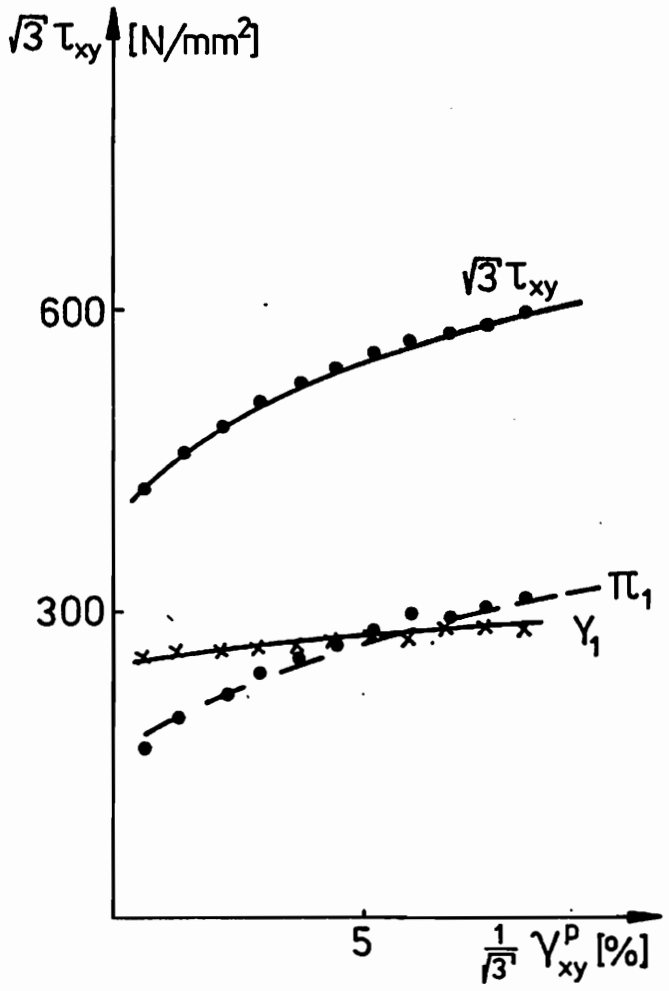

Fig.23

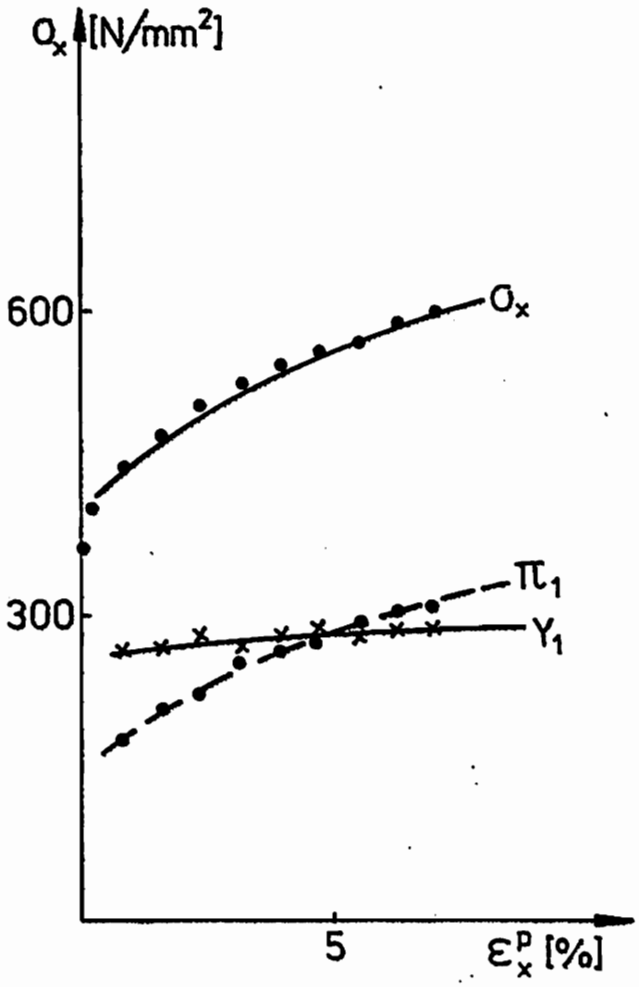

Fig. 24

Mitteilungen aus dem Institut für Mechanik

Nr. 1 Theodor Lehmann:
Große elasto-plastische Formänderungen

Nr. 2 Bogdan Raniecki/Klaus Thermann:
Infinitesimal Thermoplasticity and Kinematics of Finite Elastic-Plastic Deformations. Basic Concepts

Nr. 3 Wolfgang Krings:
Beitrag zur Finiten Element Methode bei linearem, viscoelastischem Stoffverhalten

Nr. 4 Burkhard Lücke:
Theoretische und experimentelle Untersuchung der zyklischen elastoplastischen Blechbiegung bei endlichen Verzerrungen

Nr. 5 Knut Schwarze:
Einfluß von Querschnittsverformungen bei dünnwandigen Stäben mit stetig gekrümmter Profilmittellinie

Nr. 6 Hubert Sommer:
Ein Beitrag zur Theorie des ebenen elastischen Verzerrungszustandes bei endlichen Formänderungen

Nr. 7 H. Stumpf/F.J. Biehl:
Die Methode der orthogonalen Projektionen und ihre Anwendung zur Berechnung orthotroper Platten

Nr. 8 Albert Meyers:
Ein Beitrag zum optimalen Entwurf von schnellaufenden Zentrifugenschalen

Nr. 9 Berend Fischer:
Zur zyklischen elastoplastischen Beanspruchung eines dickwandigen Zylinders bei endlichen Verzerrungen

Nr. 10 Wojciech Pietraszkiewicz:
Introduction to the non-linear theory of shells

Nr. 11 Wilfried Ullenboom:
Optimierung von Stäben unter nichtperiodischer dynamischer Belastung

Nr. 12 Jürgen Güldenpfennig:
Anwendung eines Modells der Vielkristallplastizität auf ein Problem gekoppelter elasto-plastischer Wellen

Nr. 13 Pawel Rafalski:
Minimum Principles in Plasticity

Nr. 14 Peter Hilgers:
Der Einsatz eines Mikrorechners zur hybriden Optimierung und Schwingungsanalyse

Nr. 15 Hans-Albert Lauert:
Optimierung von Stäben unter dynamischer periodischer Beanspruchung bei Beachtung von Spannungsrestriktionen

Nr. 16 Martin Fritz:
Berechnung der Auflagerkräfte und der Muskelkräfte des Menschen bei ebenen Bewegungen aufgrund von kinematographischen Aufnahmen

Nr. 17 H. Stumpf/F.J. Biehl:
Approximations and Error Estimates in Eigenvalue Problems of Elastic Systems with Application to Eigenvibrations of Orthotropic Plates

Nr. 18 Uwe Kolberg:
Variational principles and their Numerical Application to Geometrically Nonlinear v. Karman Plates

Nr. 19 Heinz Antes:
Über Fehler und Möglichkeiten ihrer Abschätzung bei numerischen Berechnungen von Schalentragwerken

Nr. 20 Czeslaw Wozniak:
Large Deformations of Elastic and Non-Elastic Plates, Shells and Rods

Nr. 21 Maria K. Duszek:
Problems of Geometrically Non-Linear Theory of Plasticity

Nr. 22 Burkhard von Bredow:
Optimierung von Stäben unter stochastischer Erregung

Nr. 23 Jürgen Preuss:
Optimaler Entwurf von Tragwerken mit Hilfe der Mehrzielmethode

Nr. 24 Ekkehard Goßmann:
Kovarianzanalyse mechanischer Zufallschwingungen bei Darstellung der mehrfachkorrelierten Erregungen durch stochastische Differentialgleichungen

Nr. 25 Dieter Weichert:
Variational Formulation and Solution of Boundary-Value Problems in the Theory of Plasticity and Application to Plate Problems

Nr. 26 Wojciech Pietraszkiewicz:
On Consistent Approximations in the Geometrically Non-Linear Theory of Shells

Nr. 27 Georg Zander:
Zur Bestimmung von Verzweigungslasten dünnwandiger Kreiszylinder unter kombinierter Längs- und Torsionslast

Nr. 28 Pawel Rafalski:
An Alternative Approach to the Elastic-Viscoplastic Initial-Boundary Value Problem

Nr. 29 Heinrich Oeynhausen:
Verzweigungslasten elastoplastisch deformierter, dickwandiger Kreiszylinder unter Innendruck und Axialkraft

Nr. 30 Franz-Josef Biehl:
Zweiseitige Eingrenzung von Feldgrößen beim einseitigen Kontaktproblem

Nr. 31 Maria K. Duszek:
Foundations of the Non-Linear Plastic Shell Theory

Nr.32 Reinhard Piltner:
Spezielle finite Elemente mit Löchern, Ecken und Rissen unter Verwendung von analytischen Teillösungen

Nr. 33 Petrisor Mazilu:
Variationsprinzipe der Thermoplastizität I. Wärmeausbreitung und Plastizität

Nr. 34 Helmut Stumpf:
Unified Operator Description, Nonlinear Buckling and Post-Buckling Analysis of Thin Elastic Shells

Nr. 35 Bernd Kaempf:
Ein Extremal-Variationsprinzip für die instationäre Wärmeleitung mit einer Anwendung auf thermoelastische Probleme unter Verwendung der finiten Elemente

Nr. 36 Alfred Kraft:
Zum methodischen Entwurf mechanischer Systeme im Hinblick auf optimales Schwingungsverhalten

Nr. 37 Petrisor Mazilu:
Variationsprinzipe der Thermoplastizität
II. Gekoppelte thermomechanische Prozesse

Nr. 38 Klaus-Detlef Mickley:
Punktweise Eingrenzung von Feldgrößen in der Elastomechanik und ihre numerische Realisierung mit Fundamental-Splinefunktionen

Nr. 39 Lutz-Peter Nolte:
Beitrag zur Herleitung und vergleichende Untersuchung geometrisch nichtlinearer Schalentheorien unter Berücksichtigung großer Rotationen

Nr. 40 Ulrich Blix:
Zur Berechnung der Einschnürung von Zugstäben unter Berücksichtigung thermischer Einflüsse mit Hilfe der Finite-Element-Methode

Nr. 41 Peter Becker:
Zur Berechnung von Schallfeldern mit Elementmethoden

Nr. 42 Dietmar Bouchard:
Entwicklung und Anwendung eines an die Diskrete-Fourier-Transformation angepaßten direkten Algorithmus zur Bestimmung der modalen Parameter linearer Schwingungssysteme

Nr. 43 Uwe Zdebel:
Theoretische und experimentelle Untersuchungen zu einem thermoplastischen Stoffgesetz

Nr. 44 Jan Kubik:
Thermodiffusion flows in a solid with a dominant constituent

Nr. 45 Horst J. Klepp:
Über die Gleichgewichtslagen und Gleichgewichtsbereiche nichtlinearer autonomer Systeme

Nr. 46 J. Makowski/L.-P. Nolte/H. Stumpf:
Finite in-plane deformations of flexible rods - insight into nonlinear shell problems

Nr. 47 Franz. K. Labisch:
Grundlagen einer Analyse mehrdeutiger Lösungen nichtlinearer Randwertprobleme der Elastostatik mit Hilfe von Variationsverfahren

Nr. 48 J. Chroscielewski/L.-P. Nolte:
Strategien zur Lösung nichtlinearer Probleme der Strukturmechanik und ihre modulare Aufbereitung im Konzept MESY

Nr. 49 Karl-Heinz Bürger:
Gewichtsoptimierung rotationssymmetrischer Platten unter instationärer Erregung

Nr.50 Ulrich Schmid:
Zur Berechnung des plastischen Setzens von Schraubenfedern

Nr. 51 Jörg Frischbier:
Theorie der Stoßbelastung orthotroper Platten und ihre experimentelle Überprüfung am Beispiel einer unidirektional verstärkten CFK-Verbundplatte

Nr. 52 W. Trampczynski:
Strain history effect in cyclic plasticity

Mitteilungen aus dem Institut für Mechanik
RUHR-UNIVERSITÄT BOCHUM
Nr. 52